Annual Review of Earth and Planetary Sciences

The Evolving Chronology of Moon Formation

Lars E. Borg[1] and Richard W. Carlson[2]

[1]Nuclear and Chemical Science Division, Lawrence Livermore National Laboratory, Livermore, California, USA; email: borg5@llnl.gov

[2]Earth and Planets Laboratory, Carnegie Institution for Science, Washington, DC, USA

Annu. Rev. Earth Planet. Sci. 2023. 51:25–52

The *Annual Review of Earth and Planetary Sciences* is online at earth.annualreviews.org

https://doi.org/10.1146/annurev-earth-031621-060538

Keywords

Moon, chronology, lunar magma ocean, giant impact, model ages

Abstract

Defining the age of the Moon has proven to be an elusive task because it requires reliably dating lunar samples using radiometric isotopic systems that record fractionation of parent and daughter elements during events that are petrologically associated with planet formation. Crystallization of the magma ocean is the only event that unambiguously meets this criterion because it probably occurred within tens of millions of years of Moon formation. There are three dateable crystallization products of the magma ocean: mafic mantle cumulates, felsic crustal cumulates, and late-stage crystallization products known as urKREEP (uniform residuum K, rare earth elements, and P). Although ages for these materials in the literature span 200 million years, there is a preponderance of reliable ages around 4.35 billion years recorded in all three lunar rock types. This age is also

observed in many secondary crustal rocks, indicating that they were produced contemporaneously (within uncertainty of the ages), possibly during crystallization and overturn of the magma ocean.

- The duration of planet formation is key information in understanding the mechanisms by which the terrestrial planets formed.
- Ages of the oldest lunar rocks range widely, reflecting either the duration of Moon formation or disturbed ages caused by impact metamorphism.
- Ages determined for compositionally distinct crust and mantle materials produced by lunar magma ocean differentiation cluster near 4.35 Gyr.
- The repeated occurrence of 4.35 Gyr ages implies that Moon formation occurred late in Solar System history, likely by giant impact into Earth.

1. INTRODUCTION

Although 50-plus years of analysis of lunar samples has provided a much clearer picture of Moon formation and differentiation, the age of the Moon has remined ambiguous. There is no question that the Moon is old, certainly over 4.36 Gyr, nor that it appears to be younger than the 4,567 Myr age of the oldest solids in the Solar System (Amelin et al. 2002, Connelly et al. 2012). How much younger, however, is an active area of debate with estimates spanning more than 200 Myr (Tera & Wasserburg 1974, Carlson et al. 2014, Borg et al. 2015, Barboni et al. 2017). Some of this confusion arises from the fact that planets need not form instantaneously, but instead develop and evolve gradually by a variety of processes until they obtain their final structure. Another complexity associated with determining the age of any planetary body is that chronologic measurements using radiometric techniques only date the time when parent and daughter isotopes were fractionated into different phases within individual rocks, or into different regional-scale to planetary-scale geochemical reservoirs. A geologic model that places the dated materials into the evolutionary timeline of a planet is therefore required to use these ages to constrain when and how the planet formed. Thus, interpreting the significance of ages determined on individual samples or sample suites changes as the petrogenetic models for their origin evolve.

Development of both geologic models for the origin of the Moon and chronometric systems to date lunar rocks occurred simultaneously. These approaches were applied to the Moon immediately after samples were first returned by the Apollo missions in 1969. This was a time shortly following the serendipitous arrival on Earth of the primitive (undifferentiated) Allende meteorite. Allende provided an ideal test sample to practice the analytical approaches that were being developed for lunar samples on a rock that dated to the earliest epochs of planet formation. Many chemical and isotopic similarities between calcium-aluminum-rich inclusions (CAIs) and some lunar rocks (e.g., anorthosites) strongly influenced ideas regarding the age of the Moon. Specific evidence that the Moon or the materials that make up the Moon were very old came with the first $^{87}Sr/^{86}Sr$ isotopic analysis when it was found that some lunar samples were not much more evolved than CAIs present in the Allende meteorite that recorded the best estimate for the initial Sr isotopic composition of the Solar System (Papanastassiou et al. 1970). The first look at lunar samples, however, dispelled the idea that the Moon formed gently and would provide relatively undifferentiated samples of the materials from which the terrestrial planets formed (Urey 1951). Instead, examination of the first lunar samples showed clearly that the Moon was born hot, perhaps even to the point where most of its crust was produced by flotation of plagioclase during solidification of a global magma ocean (Smith et al. 1970, Wood et al. 1970). Several years passed

before this hot beginning was linked to Moon formation by reaccretion of material ejected from a giant impact between a Mars-sized impactor (Theia) and the proto-Earth (Hartmann & Davis 1975). As theoretical accretion models for the terrestrial planets allow for impacts between planetary embryos to occur up to hundreds of millions of years after the beginning of the Solar System (Chambers 2004), the giant impact model for Moon formation lessened the expectation that the Moon necessarily formed during the earliest epoch of planet building.

If the Moon formed many tens to hundreds of million years after the start of Solar System formation, distinguishing chemical differentiation events associated with Moon formation from earlier events that created the chemical characteristics of the materials from which the Moon formed becomes critical. Some characteristics of lunar samples probably predate the giant impact, such as the depletion of the Moon in volatile and siderophile elements. Fortunately, cooling and crystallization of a well-stirred magma body, as predicted by global magma ocean models, offer something of an ideal situation for radiometric dating techniques because strong convection of the magma ocean mixes away any initial inherited isotopic variability in the daughter element of a radioactive decay pair. Crystallization of the magma then produces minerals with different parent/daughter elemental ratios that with time lead to measurably different isotopic compositions of daughter elements. If cooling after crystallization is relatively rapid, the formation of crystals within an igneous rock starts the radiometric clocks they contain. If the duration of both lunar accretion and crystallization of the lunar magma ocean (LMO) was short relative to the temporal resolution of the radiometric dating techniques employed, radiometric ages of LMO cumulates could provide a reasonably precise estimate for the timing of Moon formation. Here we review the most commonly invoked constraints on the age of the Moon based on volatile element depletion, core formation, LMO crystallization, and post-LMO crustal magmatism, in the context of geologic models for the origin of the dated materials.

2. AGE CONSTRAINTS FROM VOLATILE ELEMENT DEPLETION AND CORE FORMATION

Three major chemical differentiation processes (**Figure 1**) involved in early planet evolution that fractionate parent from daughter elements, and hence can potentially be dated using radioactive chronologic techniques, are (*a*) evaporation-condensation resulting in volatile-refractory element fractionation, (*b*) core formation resulting in lithophile-siderophile/chalcophile element fractionation, and (*c*) crust-mantle differentiation resulting in lithophile element fractionation. The first two of these track processes that can happen before planet formation, such as incomplete condensation of variably volatile elements from an initially hot protoplanetary disk, or core formation on planetismals that later accrete to form planets. All three can be caused by later high-temperature events driven by either endogenous energy sources, such as radioactive heating, or exogenous sources, such as the kinetic energy of major impacts. Examining when and where these events occurred in the evolutionary history of lunar materials can potentially address both what the Moon was made from and when it formed.

2.1. Volatile Element Depletion

The first analyses of lunar samples revealed that the Moon is highly depleted in volatile elements (Keays et al. 1970, Morrison et al. 1970) compared to estimates of the bulk Solar System. Early Rb-Sr isotopic analyses of the returned lunar samples (e.g., Papanastassiou et al. 1970, Compston et al. 1971) confirmed this by demonstrating that lunar samples have very low initial $^{87}Sr/^{86}Sr$ (**Figure 2*a***), testifying to derivation from materials severely depleted in the moderately volatile parent element Rb (Taylor & Norman 1990, Halliday & Porcelli 2001, Borg et al. 2022). The

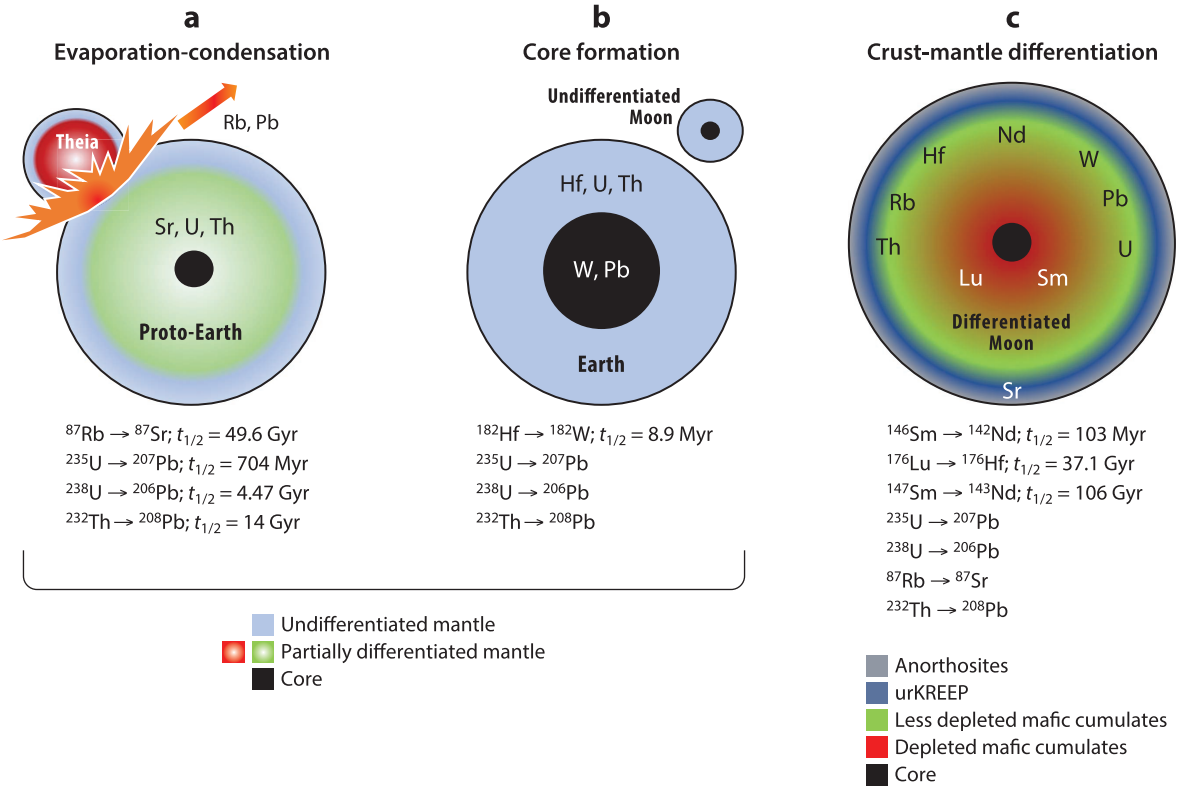

Figure 1

Diagram illustrating events that potentially fractionate parent and daughter isotopes. (*a*) Volatile-refractory element fractionation associated with the giant impact. (*b*) Lithophile-siderophile/chalcophile element fractionation associated with core formation. (*c*) Lithophile-lithophile element fractionation associated with magma ocean crystallization. Abbreviation: urKREEP, uniform residuum K, rare earth elements, and P.

ability of plagioclase to concentrate Sr, but exclude Rb, allows data for crustal anorthosites to provide the best estimate of the Sr isotopic composition of the Moon at the time of anorthosite formation (**Figure 2**). The initial Sr isotopic composition of the Moon, termed LUNI (Nyquist et al. 1974), was taken as an approximation to the initial $^{87}Sr/^{86}Sr$ of the Moon at 4.56 Gyr. Using the $^{87}Sr/^{86}Sr$ values measured recently in lunar anorthosites (**Supplemental Table 1**), the ^{146}Sm-^{142}Nd age of mare basalt source formation of 4.35 Gyr (see Section 3.2.2), and modern decay constants, the weighted average initial $^{87}Sr/^{86}Sr$ for these crustal anorthosites is 0.699056 ± 11 (2 SD). Although this value is in good agreement with the value originally proposed by Nyquist et al. (1974) of 0.69903, it represents the isotopic composition of the Moon at 4.35 Gyr, not at 4.56 Gyr (i.e., 260 Myr later).

The Rb/Sr ratio of the Sun, and hence the protoplanetary disk, is estimated from CI chondrites, which have a $^{87}Rb/^{86}Sr$ of 0.924 (Palme & O'Neill 2014) that is significantly higher than values typical of any terrestrial planet and particularly the Moon. In a reservoir (e.g., protoplanetary disk, planetesimal, planet) with CI-like Rb/Sr ratio, the $^{87}Sr/^{86}Sr$ of that reservoir will increase from the Solar System initial value of 0.698975 (Hans et al. 2013) by ~0.000138 every 10 Myr. The fact that average initial $^{87}Sr/^{86}Sr$ of lunar anorthosites is about 0.699056, and that this value is only slightly elevated compared to estimates of the Solar System initial value, means that the Moon, or the materials from which it formed, must have become volatile depleted very early in

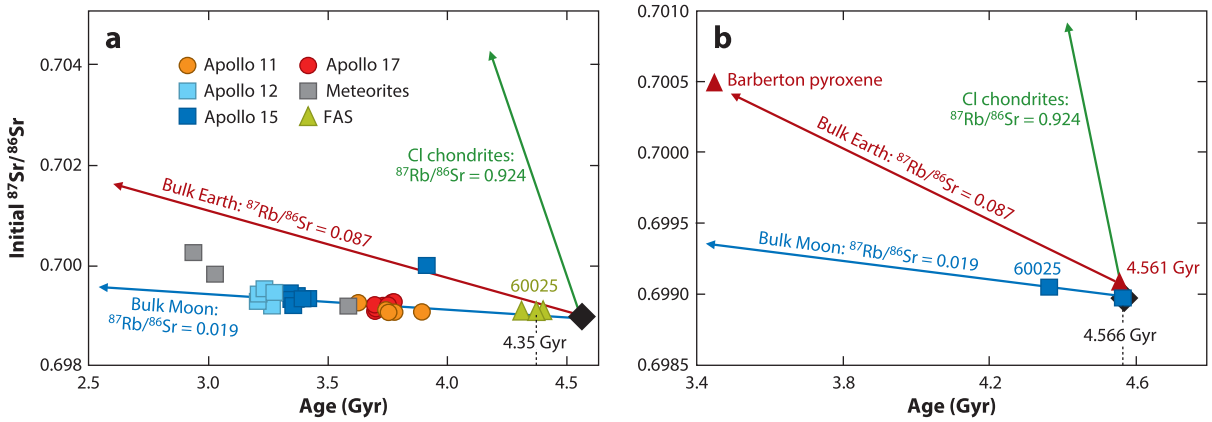

Figure 2

Sr growth curves. (*a*) The initial Sr isotopic composition of mare basalts and their model source regions that shows the low $^{87}Rb/^{86}Sr$ ratios that typify the source regions of most lunar rocks. (*b*) Sr isotope evolution of CI chondrites (*green*), the bulk Moon (*blue*), and bulk Earth (*red*) starting from the initial $^{87}Sr/^{86}Sr$ of the Solar System as estimated for CAIs (Hans et al. 2013) based on estimates for the $^{87}Rb/^{86}Sr$ (shown along the lines) for these bodies. The Rb-Sr model age calculated for the initial $^{87}Sr/^{86}Sr$ of plagioclase from anorthosite 60025 (*dark blue square*) is 4.566 Gyr while that for a pyroxene from the Barberton komatiites (*red triangle*) is 4.561 Gyr, reflecting the early volatile depletion of the materials from which both Earth and Moon formed. Abbreviations: CAI, calcium-aluminum-rich inclusion; FAS, ferroan anorthosite suite.

Solar System history. For example, Sr evolving (growing) in a reservoir starting with the Solar System initial value of 0.698975 would exceed the $^{87}Sr/^{86}Sr$ ratio observed in the anorthosites in 5.8 Myr. This is the latest possible age for volatile element depletion because it assumes that the source from which the anorthosites were derived had a $^{87}Rb/^{86}Sr$ ratio of zero from 4.561 to 4.360 Gyr. A more realistic calculation approximates the time of volatile depletion, assuming the source of the anorthosites had $^{87}Rb/^{86}Sr$ of the bulk silicate Moon of 0.019 (Newsom 1995). In this case, the evolution of the Moon is modeled to have occurred in two stages. In the first stage, Sr evolves in a reservoir with $^{87}Rb/^{86}Sr$ of CI chondrites (0.924), followed by a second stage that is assumed to have a $^{87}Rb/^{86}Sr$ of the bulk Moon (0.019). The time of the volatile element depletion event is thus modeled to occur at the onset of the second stage at 4.566 Gyr (**Figure 2*b***). A similar calculation can be done for Earth, but here the problem is finding an ancient rock with a Sr isotopic composition that reflects isotopic evolution in a reservoir with a simple prehistory prior to rock formation. One choice is the initial $^{87}Sr/^{86}Sr$ calculated for a 3.45 Gyr old pyroxene from a komatiite in the Barberton Mountains of South Africa (Jahn et al. 1982). Using an estimate of the bulk-silicate-Earth $^{87}Rb/^{86}Sr = 0.087$ (McDonough & Sun 1995), this initial Sr isotopic composition provides a model age relative to CI chondritic Rb-Sr evolution of 4.561 Gyr (**Figure 2*b***).

The great antiquity of these model ages demonstrates that the volatile element depletion of the Moon (and Earth), or the materials from which they formed, was established within just a few million years of the beginning of Solar System formation. This cannot simply reflect the separation of the refractory solids that would eventually form the terrestrial planets from the uncondensed gas of the nebula because the Rb left in that gas would continue to decay to ^{87}Sr, which would then condense into solids. If the volatile depletion of the Earth-Moon system was caused by the Moon-forming giant impact, the lunar Sr isotope data imply that the impact would have to have occurred 1–2 million years after the beginning of Solar System formation. This period is shorter than typically considered necessary for growth of planets the size of the proto-Earth

or Theia (Chambers 2004). While newer models for planet formation, such as pebble accretion (Levison et al. 2015), can accelerate planet growth, the volatile depletion of Earth and Moon is a characteristic of all of the terrestrial planets. A recent examination of this problem (Borg et al. 2022) confirms that both Theia and the proto-Earth were strongly depleted in volatile elements prior to the giant impact. Borg et al. (2022) completed several Rb-Sr evolution models in order to reproduce the $^{87}Sr/^{86}Sr$ of the bulk Moon of 0.69905 at 4.36 Gyr. If the proto-Earth is assumed to have the same $^{87}Rb/^{86}Sr$ as the present-day Earth, and Theia is assumed to have the $^{87}Rb/^{86}Sr$ of angrite meteorites (0.005), the Moon must be composed predominantly (∼90%) of material from Theia and the giant impact must be younger than ∼4.45 Gyr.

The primary implication of Rb/Sr data for lunar rocks is that the materials from which the Moon formed were volatile depleted before the Moon formed. This observation is consistent with the whole rock meteorite ^{53}Mn-^{53}Cr isochron of 4,566 ± 2.2 Myr (Qin et al. 2010) that also likely reflects separation of the more volatile Mn from more refractory Cr. As a consequence, ages based on examination of the timing of volatile-refractory element separation most likely date events occurring during the earliest stages of formation of solids in the protoplanetary disk rather than events associated with terrestrial planet and Moon formation.

2.2. Core Formation

Given the relatively small size of the core of the Moon, core-mantle separation on the Moon likely did not leave as large a chemical imprint as it did on Earth or on a differentiated planetary embryo (Theia?). For this reason, much like the case for the Moon's depletion in volatile elements, addressing whether the chemical and isotopic signatures of core formation recorded in lunar samples reflect core formation on the Moon or on the precursors from which it was derived is critical. The main radioactive chronometers sensitive to core formation are U-Th-Pb and Hf-W (**Figure 1**) because in both cases, the parent elements are lithophile whereas the daughter element is at least moderately siderophile or chalcophile. However, for the U-Th-Pb systems, untangling the role of core formation from volatile loss and Pb mobility associated with impacts is difficult due to the volatility of Pb. Both Hf and W, however, are refractory elements, so the Hf-W system should not be sensitive to the events that caused volatile depletion on the Moon (**Figure 1**). Attempts have been made to estimate the age of Moon formation by comparing the W isotopic composition of the Moon and Earth (see **Supplemental Text**) with estimates of the bulk planet Hf/W ratio of both objects (Thiemens et al. 2019). This approach depends on assumptions about the bulk W isotopic composition of both objects that are subject to considerable interpretation (e.g., Kruijer et al. 2021). The fact that modern terrestrial ocean island basalts demonstrate considerable variability in ^{182}W further complicates direct comparison of terrestrial and lunar values. Finally, it should be noted that besides being a moderately siderophile element, W is also a more highly incompatible element with respect to mantle silicate minerals than is Hf. Thus, silicate differentiation occurring during crystallization of planetary-scale magma oceans is expected to fractionate these elements, potentially superimposing an additional isotopic signal on core formation. Thus, defining a decisive lunar core formation age based on the Hf-W system has remained elusive. See the **Supplemental Text** for additional discussion of this approach.

3. AGE CONSTRAINTS FROM MAGMA OCEAN CRYSTALLIZATION

3.1. Petrogenetic Models for the Differentiation of the Moon

In terms of addressing the question of the age of a planet, the chemical differentiation that occurs through the crystallization of a magma ocean yields a strong signal that can potentially be

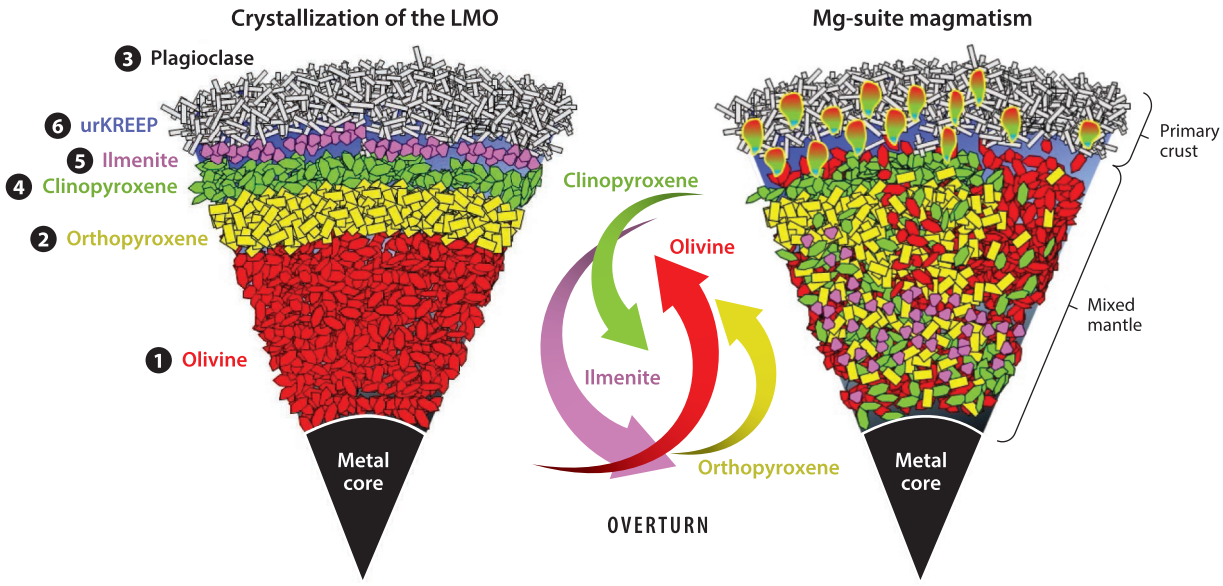

Figure 3

Diagram (not to scale) depicting early stages of lunar evolution. The initial stage is crystallization the LMO. Minerals crystallize in the order of the black circled numerals. Density-driven overturn occurs either during the last stages of crystallization or soon afterward. Ilmenite sinks and olivine rises. The final stage involves emplacement of Mg-suite magmas that have geochemical characteristics of mixtures of primary LMO cumulates. Abbreviations: LMO, lunar magma ocean; urKREEP, uniform residuum K, rare earth elements, and P.

deciphered using radioactive chronometers (**Figure 1**). To use these chronometers to date the formation of the Moon, however, several assumptions must be made: (*a*) the LMO is associated with the time of Moon formation and not some later event, such as a magma lake formed by a large impact into an already-existing Moon, (*b*) LMO crystallization occurs quickly relative to the temporal resolution of the chronometers, and (*c*) samples with a simple relationship to LMO crystallization can be found and analyzed.

Given the relatively low pressures and water contents involved even in a whole-Moon LMO, crystallization of a magma ocean of composition equal to the bulk-silicate Moon will follow a sequence well known from terrestrial layered intrusions and experimental petrology (**Figure 3**). The sequence of LMO crystallization has been extensively investigated (Walker et al. 1975, Warren 1985, Snyder et al. 1992, Elardo et al. 2011, Elkins-Tanton et al. 2011, Lin et al. 2017, Rapp & Draper 2018). These studies present a generally consistent picture that begins with crystallization of the mafic minerals olivine and orthopyroxene. If convection in the LMO is sufficiently slow, the greater density of these minerals compared to the melt will cause them to sink and accumulate at the base of the magma ocean. Removal of olivine and orthopyroxene eventually causes the remaining magma to saturate in plagioclase after 70–80% crystallization, by which time the magma is sufficiently iron-rich, and hence dense, that the plagioclase floats to form the anorthositic crust. Because this crust forms after extensive crystallization of the LMO, the rare mafic minerals in these anorthosites are iron rich, leading to the moniker ferroan anorthosites (James 1980). These rocks represent the plagioclase-rich (>90%) end-member of the ferroan anorthosite suite (FAS), which has been the focus of many chronologic investigations discussed in this section. Clinopyroxene and ilmenite crystallize after plagioclase, leaving behind highly evolved melts that contain

the elements that are not partitioned into the previously crystallized minerals. This last vestige of LMO crystallization is a highly evolved component known as urKREEP because it is a uniform residuum enriched in K, REE (rare earth elements), and P and other incompatible elements relative to all other lunar rocks (Warren & Wasson 1979). Attempts to determine the age of solidification of the LMO have therefore focused on defining the formation age of (*a*) LMO mafic cumulates, (*b*) ferroan anorthosite crust, and (*c*) urKREEP.

Two aspects of LMO evolution have important consequences for the translation of sample ages to determine the age of the Moon. First is the question of whether LMO crystallization results in a gravitationally stable sequence of cumulates or instead one with dense, iron-rich minerals near the top that will become unstable and cause an overturn of the cumulate pile (Ringwood & Kesson 1976, Elkins-Tanton et al. 2002, Parmentier et al. 2002) (**Figure 3**). Such an overturn could lead to mixing between the various layers of cumulates, as well as the possible initiation of renewed magmatism. One possible example of such magmatism is the Mg-suite crustal rocks (James 1980, Shearer et al. 2015, Borg et al. 2020, Prissel & Gross 2020) that are distinguished from FAS by the higher Mg/Fe ratio of their mafic minerals along with substantially elevated incompatible element contents due to incorporation of the urKREEP component. The Mg-suite is interpreted to be melts of the ultramafic mantle that intruded into the FAS crust (**Figure 3**). If Mg-suite magmatism was indeed caused by cumulate overturn, then their ages could provide constraints on both the duration and timing of this process. The other consequence of cumulate overturn is that it would drive mixing of the various cumulate layers, thereby blurring some of the compositional distinctions created during LMO crystallization. However, unless the mixing driven by the overturn was sufficient to erase the compositional distinctions in the lunar mantle and crust that were produced during the initial crystallization of the LMO, the cumulate overturn event could well have had minimal impact on the chronometers used to date LMO crystallization.

The second aspect of LMO evolution that is relevant to the interpretation of radiometric ages is the duration required to completely crystallize the LMO. Estimating the time needed to completely crystallize a planetary-scale magma ocean is a complex task because it depends on many parameters such as the vigor of convection; the insulating properties of a conductive crust; whether impacts broke up nascent crusts, accelerating cooling of the LMO, or instead added kinetic energy to it, prolonging LMO crystallization (Perera et al. 2018); possibly inhomogeneous radioactive heating by spatially concentrated evolved liquids (Laneuville et al. 2013); or tidal heating when the Moon was much closer to Earth shortly after its formation (Elkins-Tanton et al. 2011, Quillen et al. 2019). Early estimates that considered only radiative cooling through a conductive crust along with internal radioactive heating predicted ∼100 Myr to crystallize the majority of the LMO with residual liquids persisting for up to 500 Myr (Solomon & Longhi 1977). Similar results are seen in more recent calculations that include different parameters for the magma ocean, such as its initial depth and the viscosity of the magma (Maurice et al. 2020). In other models, the time to initiation of crust formation is as short as 1,000 years (e.g., Elkins-Tanton et al. 2011). How the duration of LMO crystallization might affect model ages for the compositionally distinct reservoirs produced by LMO crystallization also is not straightforward. For example, while urKREEP may have remained molten for up to 500 Myr (Wieczorek & Phillips 2000), its chemical characteristics may not have changed significantly during this interval because further differentiation was likely hampered by the difficulty associated with removing crystals from a small volume of highly fractionated melt. In this case, the model age for urKREEP formation will more closely approximate the time of initial formation of the compositional characteristics of this component rather than the time it finally solidified.

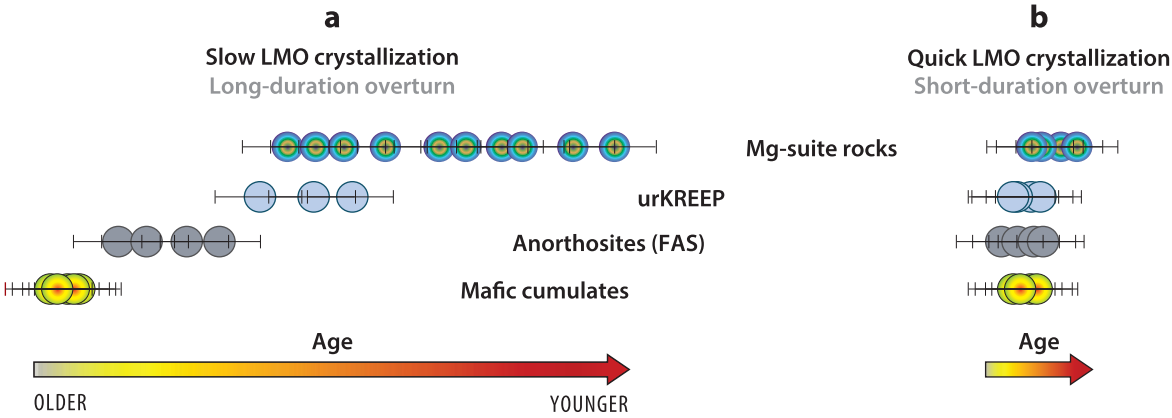

Figure 4

Schematic illustrating the expected range of ages for (*a*) a slow-cooled LMO followed by a prolonged period of overturn producing Mg-suite magmas and (*b*) a quickly cooled LMO that is contemporaneous or closely followed by overturn and Mg-suite magmatism. Abbreviations: FAS, ferroan anorthosite suite; LMO, lunar magma ocean; urKREEP, uniform residuum K, rare earth elements, and P.

The consequences of these different cooling and dynamic models for the evolution of the LMO could thus potentially impact the chronological results for lunar samples in the following ways:

- If magma ocean crystallization was prolonged for a hundred million years or longer, one might expect a measurable age range in crustal anorthosites, as well as a potentially resolvable age difference between the various LMO crystallization products. In this case, the expected chronological stratigraphy would result in initial formation of mafic cumulate mare basalt sources, FAS crust next, and urKREEP the youngest (**Figure 4*a***).
- If the magma ocean crystallized quickly (less than a few tens of millions of years), FAS crustal rocks should all have essentially the same age, within analytical resolution, and that age should be the same as other LMO cumulates such as the mafic cumulate source rocks of mare basalts and urKREEP (**Figure 4*b***).
- If cumulate overturn occurred within a few million years of LMO crystallization, it likely would have little or no signature in the chronological data for lunar samples (**Figure 4*b***). If overturn was prolonged and induced magmatism (i.e., the Mg-suite), a resolvable range in the crystallization ages of those magmas would record the duration of the overturn (**Figure 4*a***).

These expectations are tested through examination of the lunar data in the following sections.

3.2. Differentiation Age of the Moon

Understanding the age of differentiation on the Moon is complicated by the numerous investigations completed on lunar samples since the late 1960s that have yielded conflicting results. The discussion below attempts to present the most coherent set of ages that appear to be both robust and compliant with the basic petrologic constraints provided by the LMO model of differentiation. We are not attempting to review every age determination completed since the Apollo program first returned samples from the Moon. For this the reader is referred to reviews by Nyquist & Shih (1992), Borg et al. (2015), and Papike et al. (2018).

3.2.1. The age of mafic lunar magma ocean cumulates. A key observation arguing for a relatively young age for the Moon is that lunar samples show no isotopic variability in a variety

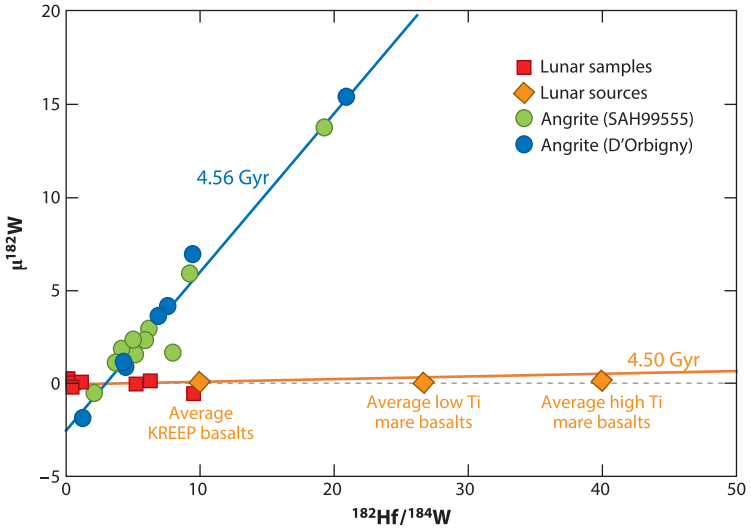

Figure 5

Hf-W data for lunar samples and average mare basalt subgroups from Touboul et al. (2007, 2009, 2015) demonstrating no variability in ^{182}W, indicating the ^{182}Hf-^{182}W system was not alive when the source regions of these lunar lithologies formed. This defines a maximum age of LMO crystallization of 4.50 Gyr (Kruijer & Kleine 2017). Data for 4.56 Gyr angrites SAH99555 and D'Orbigny are shown for comparison (Markowski et al. 2007). Abbreviations: KREEP, K, rare earth elements, and P; LMO, lunar magma ocean.

of short-lived radioactive systems that have been used effectively to date meteorites that formed within tens of millions of years of Solar System formation. Studies of lunar samples have so far not identified any variability in Mg (Sedaghatpour et al. 2013), Cr (Lugmair & Shukolyukov 1998), or W (Kruijer et al. 2015, Touboul et al. 2015) isotopic composition that can be attributed to the decay of ^{26}Al ($t_{1/2}$ = 0.7 Myr), ^{53}Mn ($t_{1/2}$ = 3.7 Myr), or ^{182}Hf ($t_{1/2}$ = 8.9 Myr) despite the fact that crystallization of the LMO is predicted to strongly fractionate these parent-daughter pairs. Instead, small variations in ^{26}Mg, ^{53}Cr, and ^{182}W isotopic compositions that have been reported in lunar samples have been attributed to either mass-dependent igneous processing or production by nuclear reactions that occur in response to bombardment by energetic cosmic rays (Leya et al. 2000, Touboul et al. 2007, Sedaghatpour et al. 2013, Bonnand et al. 2016). Given the abundance of samples representing and containing various differentiation products of the LMO, this observation indicates that the radioactive parents of these isotopes were extinct when the Moon underwent differentiation associated with crystallization of the LMO.

The measurement of significant variability of W isotopic composition in ancient, differentiated meteorites leading to the production of Hf-W isochrons (**Figure 5**) demonstrates that the Hf-W system can provide precise age constraints on planetesimal-scale differentiation events if they occurred within a few million years of Solar System formation. The fact that there is no measurable variability in W isotopic composition in lunar samples that can be attributed to the decay of ^{182}Hf (**Figure 5**) provides a maximum age limit for the crystallization of the LMO. Although the first high-precision W isotope analyses of lunar rocks found significant variability in the ^{182}W/^{184}W ratio (Lee et al. 1997, 2002; Leya et al. 2000; Kleine et al. 2005), this variability was eventually attributed to cosmic ray irradiation that created ^{182}W by neutron capture on ^{181}Ta (Leya et al. 2000). Later work that concentrated on analyzing only metals separated from lunar samples that did not contain ^{182}W generated from ^{181}Ta (Touboul et al. 2007, 2009, 2015) or corrected for the cosmogenic ^{182}W production (Kruijer et al. 2015, Kruijer & Kleine 2017) found no variability

in $^{182}W/^{184}W$ within measurement uncertainty (**Figure 5**). As their sample suite included mare basalts, KREEP- (K, rare earth elements, and P) rich samples, and ferroan anorthosites, the time constraints provided by Hf-W do not track lunar core formation, but rather magma ocean differentiation that led to the production of these distinct sources and rock types. Given the unresolved variation in $^{182}W/^{184}W$ of these samples, despite large differences in Hf/W estimated for their sources, the slope of the Hf-W isochron for the lunar samples is zero (**Figure 5**). Including the uncertainties on the data, Touboul et al. (2007) estimated the maximum age of LMO crystallization to be 4.51 Gyr. This was revised downward slightly by Kruijer & Kleine (2017) to a little less than 4.50 Gyr. Lunar Hf-W systematics thus show only that the formation of the chemically distinct sources of the various lunar igneous rock types occurred after ^{182}Hf had become extinct, and hence provide only an upper limit to the time of magma ocean differentiation of 4.50 Gyr.

The most widely applied short-lived system for lunar studies is based on the decay of ^{146}Sm to ^{142}Nd with a half-life of 103 Myr (e.g., Nyquist et al. 1995, Boyet & Carlson 2007, Brandon et al. 2009, McLeod et al. 2014, Borg et al. 2019). **Figure 6** is a compilation of all the data reported for mare basalts. The data from the various investigations are generally similar, although the Sm-Nd isotopic systematics were determined using different mass spectrometry techniques and different isotopic tracers, and were corrected for neutron capture using different algorithms. As seen in **Figure 6**, there is only a small amount of variation (about 50 ppm) in $^{142}Nd/^{144}Nd$ in all the mare basalts. Thus, like other short-lived isotope systems mentioned previously, LMO differentiation occurred sufficiently late in Solar System history that the ^{146}Sm-^{142}Nd isotope system was approaching extinction. In contrast, martian basalt sources plotted on **Figure 6** demonstrate about twice as much variation in $^{142}Nd/^{144}Nd$ as the lunar basalt sources, despite having slightly less variation in $^{147}Sm/^{144}Nd$, indicating that Mars underwent planetary differentiation significantly earlier than the Moon.

In order to estimate the formation age of their mantle source regions, the $^{142}Nd/^{144}Nd$ measured in mare basalts are plotted versus the $^{147}Sm/^{144}Nd$ calculated for their mantle source regions using the measured $^{143}Nd/^{144}Nd$ ratios (for derivations of the appropriate equations, see Nyquist et al. 1995, Borg et al. 2016). This alleviates much of the uncertainty associated with fractionation of Sm from Nd during production of the basaltic parental magmas by partial melting much later in lunar history. Furthermore, ages obtained using this approach are independent of the initial $^{142}Nd/^{144}Nd$ ratio of the Moon. The weighted average age reported for the formation of the mare basalt source regions by all lunar investigations (Nyquist et al. 1995, Rankenburg et al. 2006, Boyet & Carlson 2007, Brandon et al. 2009, McLeod et al. 2014, Borg et al. 2019) is 4,336 ± 8 Myr (uncertainty is 2 SD). Lunar basaltic meteorites, as well as FAS crustal cumulates (Borg et al. 2011, Boyet et al. 2015), plot in the field defined by the Apollo mare basalts, demonstrating that samples from widespread locations on the Moon and produced in different stages of LMO crystallization were derived from isotopically indistinguishable sources at the same time. This suggests that the ^{146}Sm-^{142}Nd isochron records differentiation on a global scale as is predicted by the LMO model of lunar differentiation.

3.2.2. The age of the anorthositic crust. The FAS makes up the majority of the lunar crust. It is thought to be a flotation cumulate produced after 70–80% solidification of the LMO (Snyder et al. 1992, Elkins-Tanton et al. 2011, Rapp & Draper 2018). As a consequence, ferroan anorthosite ages should approximate the age of LMO crystallization at the point of plagioclase saturation. Numerous attempts have been made to determine crystallization ages of ferroan anorthosites using the Rb-Sr, U-Pb, and Sm-Nd isotope systems. The Rb-Sr system has not yielded coherent isochron ages due to mobilization of Rb during impact metamorphism (**Supplemental Text**).

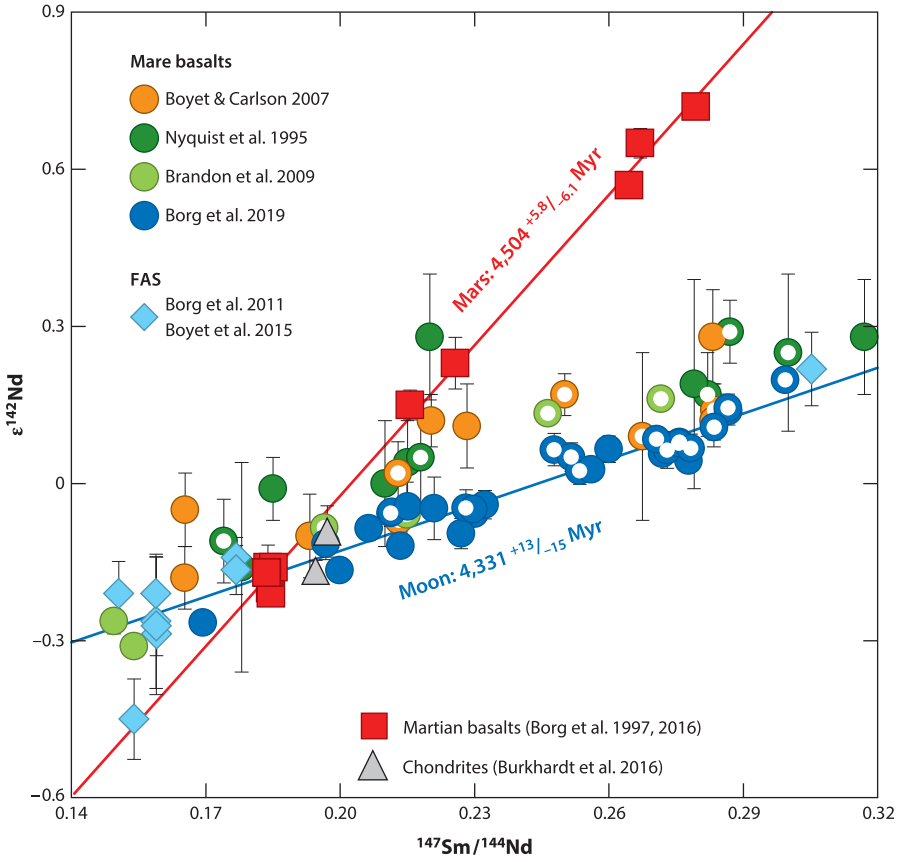

Figure 6

Epsilon ^{142}Nd–^{147}Sm/^{144}Nd model isochron showing ages of silicate differentiation on Mars and Moon. White circles inside mare basalt data points represent samples that require little correction for neutron capture defined by measured ε^{149}Sm less than 6. Data from Borg et al. (1997, 2011, 2016, 2019), Boyet et al. (2015), and Burkhardt et al. (2016) used the same mass spectrometry methods and Sm-Nd isotopic tracers and are directly comparable. The red line is a regression through martian data yielding an age of 4,504 $^{+5.8}/_{-6.1}$ Myr, and the blue line is a regression through mare basalt data (*dark blue circles*) yielding an age of 4,331 $^{+13}/_{-15}$ Myr. The average age determined by all investigations for the formation of the mare basalt source regions is 4,336 ± 8 Myr. Note that the older age of differentiation on Mars compared to the Moon is reflected in the fact that martian meteorites demonstrate about twice as much variation in ^{142}Nd than lunar samples despite demonstrating similar ranges in ^{147}Sm/^{144}Nd. Abbreviation: FAS, ferroan anorthosite suite.

Attempts to date FAS samples have also employed the U-Pb chronometer, generally with similarly limited success. As discussed in detail in the **Supplemental Text**, the U-Pb isotopic system in these ancient samples is heavily contaminated by both terrestrial Pb and Pb characterized by elevated ^{207}Pb/^{206}Pb and low ^{204}Pb/^{206}Pb ratios (e.g., Tera et al. 1974, Hanan & Tilton 1987, Premo et al. 1989). The high ^{207}Pb/^{206}Pb component has been identified in leachates in mineral separates and is isotopically similar to both Apollo 16 soils (Tera & Wasserburg 1972, Nunes et al. 1973) and the Apollo 15 anorthosite 15415 (Tera et al. 1974), leading to the suggestion that it might represent a lunar contaminant mobilized as a result of a major impact into the lunar surface at 3.9 Gyr (see **Supplemental Text**).

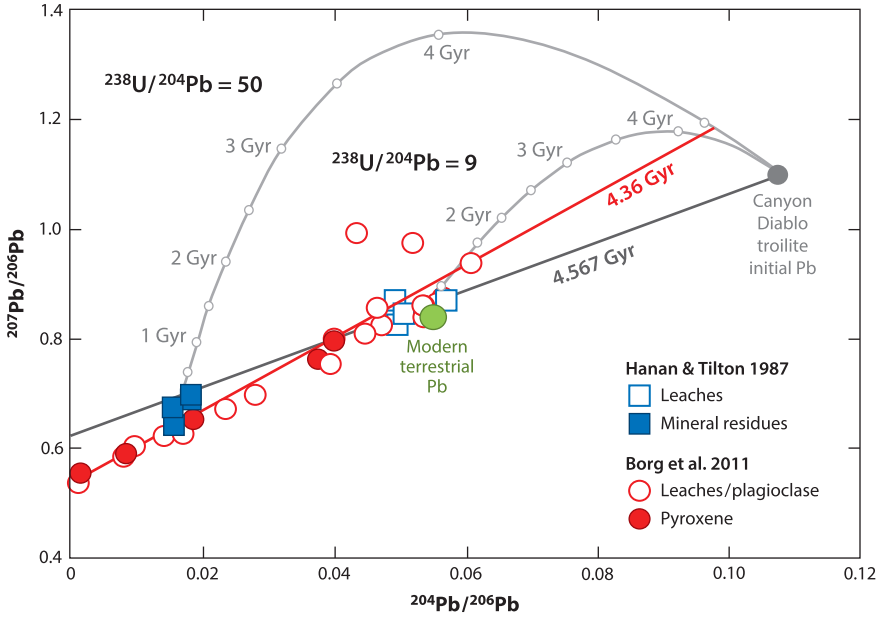

Figure 7

Pb-Pb isochron diagram for minerals and their leaches from Apollo 16 anorthosite 60025. Two Pb isotope growth curves are shown for $^{238}U/^{204}Pb = 9$ and 50. The dark gray line is the 4.567 Gyr isochron. The red line is fit through only the data for the leached minerals from Borg et al. (2011). The composition of modern terrestrial Pb (Stacey & Kramers 1975) is shown by the green circle.

There have been two studies that reported Pb-Pb ages of FAS samples. Although both ages are determined on sample 60025, they are substantially different. Hanan & Tilton (1987) calculated Pb-Pb and U-Pb model ages on three plagioclase-rich bulk samples that averaged 4.51 ± 0.01 Gyr (**Figure 7**). The 4.51 Gyr U-Pb model age was calculated assuming the Pb incorporated into the plagioclase during crystallization had the same isotopic composition as Solar System primordial Pb as represented by the Pb isotopic composition measured for troilite in the Canyon Diablo iron meteorite. The Pb-Pb age was defined by a line regressed through the three 60025 whole rocks and Canyon Diablo Pb. The assumption that primordial Pb with the isotopic composition of Canyon Diablo troilite was present on the Moon at 4.51 Gyr is challenged by many investigations that conclude the Moon has a high $^{238}U/^{204}Pb$ ratio (Tera et al. 1974, Premo et al. 1989), possibly over 1,000 (Snape et al. 2016) compared to a Solar System value of 0.19 or a bulk terrestrial value of 8–9 (Stacey & Kramers 1975). This high U/Pb of the Moon would result in it having much more radiogenic Pb isotopic composition than Canyon Diablo at the time 60025 formed, which would lead to a younger calculated age for the data reported by Hanan & Tilton (1987).

Borg et al. (2011) performed sequential washing steps to remove Pb contamination present on plagioclase and pyroxene minerals from 60025, resulting in leached fractions with lower $^{204}Pb/^{206}Pb$ ratios (**Figure 7**). Despite substantial washing, progressively digested plagioclase fractions still demonstrated evidence for disturbance of the U-Pb system, with much of the data deviating from the line defined by the leached mafic fractions in the direction of terrestrial Pb (**Figure 7**). In contrast, some progressively digested pyroxene mineral fractions yielded Pb isotopic compositions with $^{204}Pb/^{206}Pb$ values near zero. An isochron regressed through these data points intersects the y-axis at a $^{204}Pb/^{206}Pb$ value corresponding to an age of 4,359 ± 2 Myr with

a source $^{238}U/^{204}Pb$ of 15. While the data with the lowest $^{204}Pb/^{206}Pb$ are so close to purely radiogenic Pb that changes in the slope of the line fit to the data would have little consequence for the calculated age, the fact that the line extrapolates to an initial Pb isotopic composition indicating a source $^{238}U/^{204}Pb$ of ∼15 is consistent with that determined for other highlands samples (Edmunson et al. 2009) and shows that ages calculated assuming initial Pb equal to primordial Pb will overestimate the true crystallization age.

The only chronometer that yields even semi-coherent isotopic systematics when applied to FAS samples is the Sm-Nd isotopic system. As a consequence, it has proven to be the most reliable mechanism with which to obtain useful age information. There have been eight attempts to date FAS samples using this isotopic system (Carlson & Lugmair 1988; Alibert et al. 1994; Borg et al. 1999, 2011; Norman et al. 2003; Nyquist et al. 2006; Marks et al. 2019; Sio et al. 2020). Although all the investigations have yielded linear arrays of data on Sm-Nd isochron plots, the slopes correspond to a wide range of ages from 4.29 to 4.57 Gyr (**Supplemental Table 1**). However, the Sm-Nd data indicate that many of the corresponding ages have characteristics suggesting they may not represent the crystallization ages of the sample (see the discussion on assessing the reliability of Sm-Nd ages in the **Supplemental Text**). For example, 62236 has a very large positive initial $\varepsilon^{143}Nd$ value, whereas 67016 and 67215 and one 60025 age determination have moderately high values. Given that the Moon and the materials from which it formed likely have nearly flat (chondritic) REE patterns, the elevated initial $\varepsilon^{143}Nd$ of these ancient samples is not obviously consistent with petrologic understanding of the formation of the FAS. Likewise, the isochrons for samples 67016 and 67215 have very large uncertainties and large mean square of weighted deviates (MSWDs), suggesting disturbance of their Sm-Nd systematics. The FAS clast from 60016 has a very well-defined age of 4.30 Gyr but exhibits a texture indicative of very slow cooling so that concordant Sm-Nd and Ar-Ar ages have been interpreted to reflect the time the sample was excavated from depth rather than crystallization (Marks et al. 2019). Three samples, 60025, 62237, and Y-86032, analyzed by Borg et al. (2011), Sio et al. (2020), and Nyquist et al. (2006), yield Sm-Nd isochrons with relatively low uncertainties and MSWDs and have initial $\varepsilon^{143}Nd$ values consistent with petrologic models for the origin in FAS as LMO flotation cumulates. However, only 60025 has concordant ages defined by multiple isotopic systems including the ^{147}Sm-^{143}Nd, ^{146}Sm-^{142}Nd, and Pb-Pb chronometers. The average age of 60025 is 4,360 ± 3 Myr and provides the tightest age constraint on formation of a FAS sample. The weighted average age of all three samples is 4,361 ± 21 Myr (uncertainty is 2 SD) and probably provides the best estimate for the timing and duration of FAS magmatism currently available.

3.2.3. KREEP model ages. Model ages published for urKREEP are based on the Rb-Sr, Sm-Nd, or Lu-Hf isotopic systematics of lunar samples. These are model ages because they provide estimates of the time that parent and daughter isotopes were fractionated during solidification of the LMO from a Moon that is assumed to be undifferentiated. One implicit assumption of these model ages is therefore that the initial isotopic composition of the bulk Moon is known so that the first stage (from Moon formation to urKREEP formation) of primordial lunar isotopic evolution can be predicted. Another assumption is that the isotopic evolution of urKREEP can be deduced from the samples so that the second stage (from urKREEP formation to the present day) of isotope evolution of urKREEP can be calculated. Both of these assumptions are subject to uncertainties that will affect the model age calculated as discussed in the **Supplemental Text**. In the case of the Rb-Sr system, Rb can be mobilized by impact metamorphism leading to inaccurate sample Rb/Sr ratios. Attempts to correct for this phenomenon resulted in Rb-Sr model ages for KREEP-rich highlands samples that range from 4.25 to 4.42 Gyr (Palme 1977, Nyquist & Shih 1992).

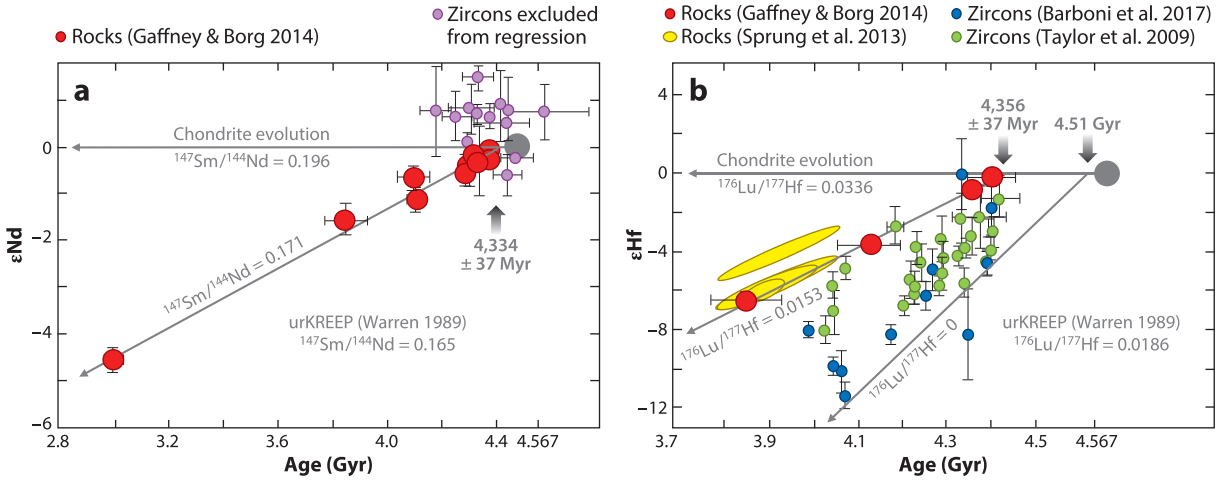

Figure 8

Age versus initial isotopic composition diagram of KREEP-rich samples. Model ages are defined by the intersection of chondritic isotopic evolution curves and lines regressed through the measured data. The slope of the regressed line is proportional to the parent/daughter ratio of urKREEP and therefore can be used to evaluate the model. Abbreviations: KREEP, K, rare earth elements, and P; urKREEP, uniform residuum K, rare earth elements, and P.

For more impact-resistant isotopic systems, such as Sm-Nd and Lu-Hf, ages are calculated by projecting the isotopic evolution of KREEP-rich samples backward until they match the isotopic composition of the undifferentiated Moon at a common point in time (see discussion in Lugmair et al. 1976). The average urKREEP model age determined using the Sm-Nd isotopic compositions of three KREEP-rich impact breccias and one KREEP basalt (15382) by Lugmair & Carlson (1978) and Carlson & Lugmair (1979) is 4.32 ± 0.03 Gyr (when calculated using modern values for lab standards and average chondrite Sm-Nd evolution in Bouvier et al. 2008). Note that these model ages depend on how closely the measured Sm/Nd ratios of the samples approach that of the urKREEP reservoir.

More recent approaches to determine the age of formation of urKREEP have circumvented the need to know the $^{147}Sm/^{144}Nd$ evolution of urKREEP by adopting a graphical approach in which whole rocks are plotted on a *T* (age) versus *I* (initial) isotope diagram (**Figure 8**). The urKREEP model age is defined by the intersection of a line regressed through the data for KREEP-rich samples of different ages with the modeled isotopic evolution of the bulk, undifferentiated Moon. A plot of Sm-Nd ages and initial isotopic compositions of urKREEP-rich basalts and Mg-suite rocks compiled by Borg et al. (2015) demonstrates significant scatter so that no obvious model age is defined. This reflects the highly variable quality of the Sm-Nd data, illustrated by the observation that multiple analyses of the same samples often do not yield Sm-Nd ages or initial Nd isotopic compositions that agree within uncertainty (see Section 4.1). However, if only isochrons yielding ages with low uncertainty and low MSWDs are used, a linear relationship is observed that defines a line that intersects chondritic evolution at 4,334 ± 37 Myr (**Figure 8*a***). The fact that the slope of the regression corresponds to a growth curve with a $^{147}Sm/^{144}Nd$ of 0.171 that closely matches estimates of urKREEP of 0.163–0.168 based on analysis of samples (Lugmair & Carlson 1978, Warren 1989) suggests that this is the best urKREEP model age defined by the current Sm-Nd data.

A similar plot can be derived for the Lu-Hf system (**Figure 8*b***). Hafnium data require significant correction for the capture of epithermal neutrons that was not accounted for in the earliest Hf

measurements of lunar samples, so that only the most recent Hf isotopic data are discussed here. Initial ε^{176}Hf values calculated from whole rocks with known ages and corrected for epithermal neutron capture effects define a line corresponding to a model age of 4,356 ± 37 Myr (Sprung et al. 2013, Gaffney & Borg 2014). The ^{176}Lu/^{177}Hf defined by the regression is 0.015 and is reasonably close to estimates of urKREEP of 0.018 (e.g., Warren 1989), suggesting the regression accurately represents the growth of urKREEP. If initial ε^{176}Hf values calculated from individual zircons analyzed by Taylor et al. (2009) and Barboni et al. (2017) that are most likely derived from KREEP-rich samples are included on the plot, there is considerably more scatter. These data therefore cannot be used to define an age through regression analysis. These authors instead defined a urKREEP model age of 4.51 ± 0.01 (1 sigma) Gyr by assuming that urKREEP had a ^{176}Lu/^{177}Hf ratio of zero and that this growth curve passed through the zircon with the least radiogenic Hf isotopic composition at a given age. Using this approach, but assuming that the source of the rocks that crystallized these zircons had a Lu/Hf ratio similar to urKREEP yields model ages older than the Solar System for many of the analyzed zircons. Thus, the most geologically reasonable age determinations for urKREEP are defined by regression through the whole-rock data. In this case, the weighted average urKREEP model age determined by regression of the Sm-Nd and Lu-Hf data is 4,345 ± 26 Myr.

3.3. Evaluation of Ages of Lunar Magma Ocean Cumulates

There are essentially no discernable differences in the range of ages determined for crystallization of various LMO cumulates (**Figure 9**) including mafic cumulates (4,336 ± 8 Myr), FAS felsic cumulates (average FAS = 4,361 ± 21 Myr; 60025 = 4,360 ± 3 Myr), and urKREEP (4,345 ± 26 Myr), providing confidence that they record the fractionation of parent and daughter isotopes associated with the crystallization of the LMO. These ages rely on three distinct chronological approaches whose sensitivity to interpretational assumptions would not obviously drive the ages to overlap with one another. The age for urKREEP is a model age that assumes that the Moon was evolving with chondritic Sm/Nd and Lu/Hf prior to formation of the urKREEP reservoir. Maurice et al. (2020) point out that if the latter stages of LMO crystallization were prolonged for more than 100 Myr and the parental magma of urKREEP was evolving to increasingly subchondritic Sm/Nd and Lu/Hf during this interval, the model ages for urKREEP when calculated with respect to chondritic evolution would underestimate the urKREEP formation age, pushing the age of urKREEP to 4.19–4.27 Gyr. This possibility seems unlikely given that Mg-suite rocks that carry a urKREEP trace element signature have crystallization ages older than 4.27 Gyr (**Figure 9**; **Supplemental Table 2**). The model age for the mare basalt source region is a whole rock ^{146}Sm-^{142}Nd isochron that depends less on assumptions about pre-LMO lunar isotopic evolution than does the urKREEP model age. The whole rock isochron approach does depend on the assumption that all the rocks that define this isochron derive from sources that at one time had the same Nd isotopic composition and that one can accurately correct for the parent-daughter elemental fractionation that happened during the much later melting that resulted in mare basalt magmatism. Not accounting for this fractionation can lead the whole rock isochrons to give inaccurately older ages (**Supplemental Text**). The ages for FAS cumulates are true internal isochron ages whose largest uncertainty is whether the ages record the crystallization of the samples or instead their prolonged cooling deep in the crust or resetting/disturbance by later impact events. Although the interpretational uncertainties in the different chronological approaches used would drive the ages in different directions, ages for all three LMO units overlap between 4,336 and 4,361 Myr, suggesting differentiation of the LMO took no more than about 25 Myr (**Figure 10**). The chronology therefore supports a LMO model in which lunar differentiation was relatively rapid (**Figure 4*b***). The concordance between the ages of LMO cumulates further suggests that post-crystallization

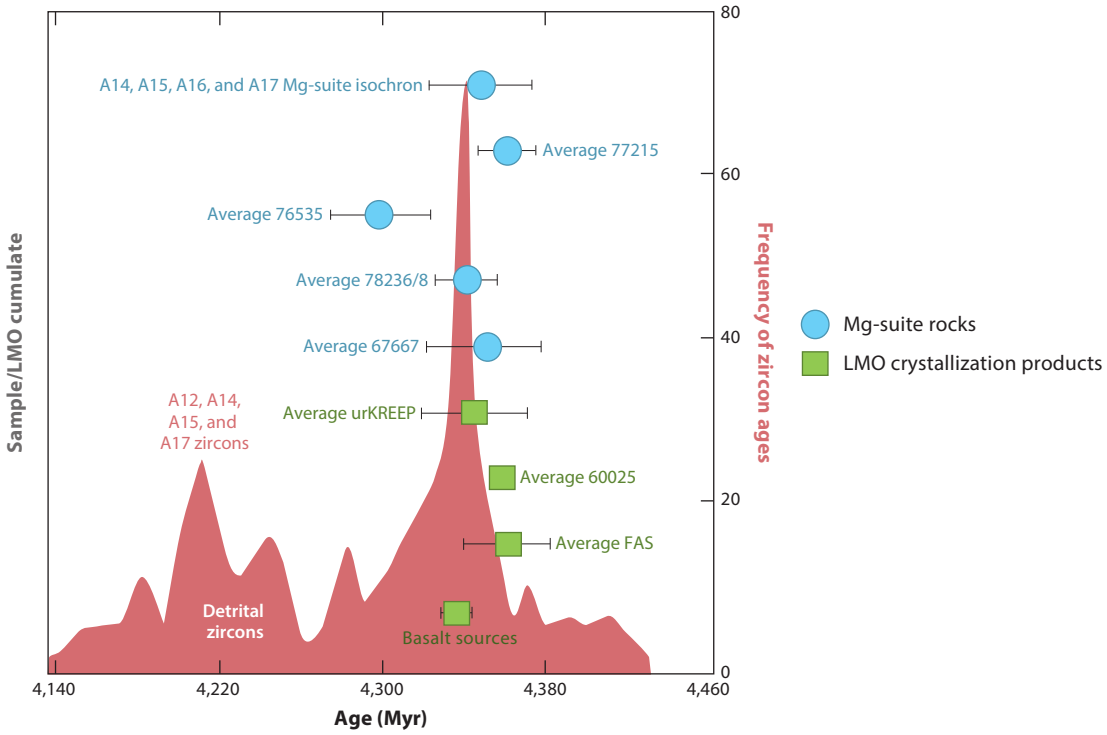

Figure 9

Summary of ages for LMO crystallization products, Mg-suite rocks, and detrital zircons. Data sources for rocks and LMO cumulates are cited in the text. Data for zircons are from Grange et al. (2009, 2011), Meyer et al. (1996), Nemchin et al. (2006; 2008; 2009a,b), Pidgeon et al. (2007), Taylor et al. (2009), and Barboni et al. (2017). Abbreviations: FAS, ferroan anorthosite suite; LMO, lunar magma ocean; urKREEP, uniform residuum K, rare earth elements, and P.

isotopic re-equilibration of the mare basalt source regions, as might be expected from wholesale overturn and melting of primordial cumulates, did not occur.

Although we feel that these ages are the most representative of the time of formation of LMO cumulates that are currently available, they almost certainly provide only a snapshot of LMO crystallization. For example, the average FAS age of 4,361 ± 21 Myr is based on only three samples, two of which are from the Apollo 16 landing site. Thus, the period of global FAS crystallization might be more extended than is represented by the average age presented here. Likewise, the ^{146}Sm-^{142}Nd age of the mare basalt sources is robust in the sense that it has been confirmed by multiple investigations. However, the ^{146}Sm half-life has been measured several times, yielding values ranging from 68 Myr to 103 Myr (Meissner et al. 1987, Kinoshita et al. 2012). Although a comparison of ^{146}Sm-^{142}Nd isochron ages with the U-Pb and ^{147}Sm-^{143}Nd ages determined on the same samples indicates the half-life of 103 Myr yields more concordant results than the 68 Myr half-life (Marks et al. 2014), the rate of decay of ^{146}Sm is not as well established as it is for other parent isotopes used to date crystallization of LMO cumulates. Using the half-life suggested by Kinoshita et al. (2012), the 4,336 Myr age for the mare basalt source quoted above would be 4,416 Myr. Of all the ages, the urKREEP model ages are arguably the most reliable. The model ages are defined by numerous KREEP-rich igneous samples that have been analyzed (except detrital zircons) and are concordant for both the Sm-Nd and Lu-Hf systems. Thus, this LMO chronology is internally coherent and provides a temporal framework of planetary evolution

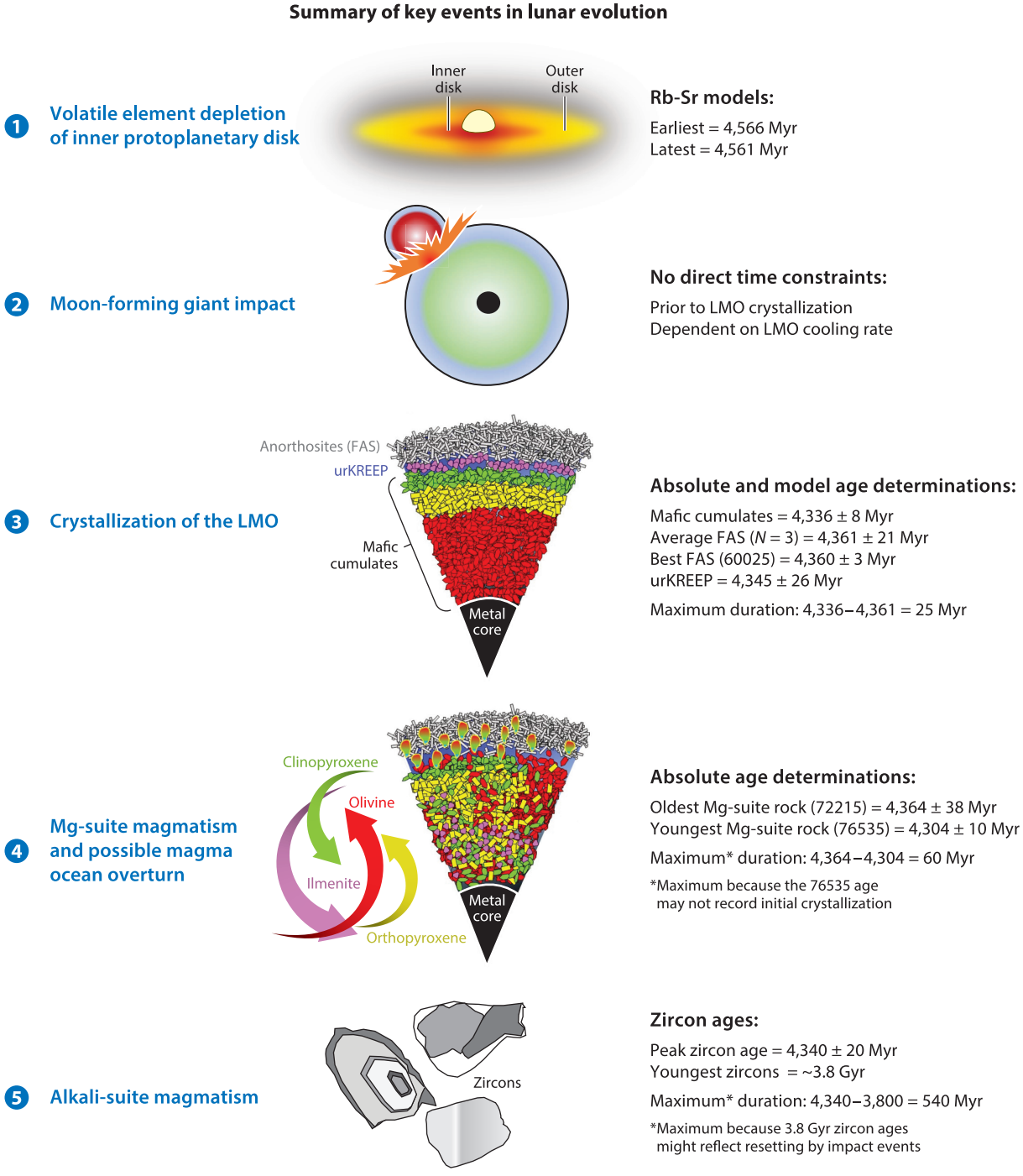

Figure 10

Diagram illustrating key events in the evolution of Moon. Ages of events are discussed in the text. Abbreviations: FAS, ferroan anorthosite suite; LMO, lunar magma ocean; urKREEP, uniform residuum K, rare earth elements, and P.

that is compatible with LMO evolution scenarios derived independently from geochemical and experimental petrology investigations (e.g., Longhi 1977, Snyder et al. 1992, Shearer et al. 2006, Elkins-Tanton et al. 2011, Lin et al. 2017, Rapp & Draper 2018).

4. AGE CONSTRAINTS FROM OTHER HIGHLAND ROCK SUITES

The lunar crust is composed of three suites of crustal rocks: the FAS, Mg-suite, and alkali-suite. As discussed above, the first, and presumably oldest, is the FAS, which represents primordial LMO cumulate crust. The second is the Mg-suite that contains Ca-rich plagioclase accompanied by high proportions of Mg-rich olivine (troctolites) and Mg-rich orthopyroxenes (norites). The remaining group is the alkali-suite. This suite of rocks is predominantly composed of evolved felsites and granites (e.g., Brown et al. 1972), with minor amounts of quartz monzodiorites (Warren & Wasson 1980). This suite is the source of lunar zircons found in lithic breccias and soils. Below we discuss the temporal relationship of these rock suites with respect to LMO crystallization.

4.1. Ages of the Mg-Suite

The Mg-suite appears to be derived from three LMO cumulate reservoirs (e.g., Shearer et al. 2006, 2015). The first is the olivine- and pyroxene-rich mafic cumulates produced in the early stage of LMO solidification. These are characterized by high Mg concentrations and Mg/Fe ratios. The second component appears to be similar to plagioclase-rich cumulates of the FAS suite. This component is characterized by anorthositic plagioclase with strongly elevated Ca contents. The third component is urKREEP, which imparts an enriched incompatible element signature on these rocks. Like all highland samples, only a few (about 8) Mg-suite samples have been identified that are amenable to isotopic dating (see reviews in Nyquist & Shih 1992; Snyder et al. 1995a, 2000; Nyquist et al. 2001; Shearer et al. 2006; Borg et al. 2015; Papike et al. 2018). Ages reported for the Mg-suite rocks range widely from 4.16 to 4.57 Gyr and are listed in **Table 2** (**Supplemental Text**). About half of the ages determined on these rocks are defined by single chronometers, have large uncertainties and MSWDs, and have not been successfully confirmed by multiple investigations (Borg et al. 2015). For example, a Sm-Nd age of 4.18 ± 0.07 Gyr was reported for feldspathic lherzolite 67667 by Carlson & Lugmair (1981), whereas Borg et al. (2020) determined concordant Sm-Nd and Rb-Sr ages of 4.35 ± 0.03 and 4.37 ± 0.07 Gyr. Likewise, clast B from lithic breccia 15445 has yielded ages ranging from 4.29 to 4.47 Gyr (Shih et al. 1993, Gaffney et al. 2015). There are even outlying ages for relatively well-dated samples such as the related norites 78236 and 78238. Whereas most chronological studies (Carlson & Lugmair 1981, Edmunson et al. 2009, Zhang et al. 2021) measure ages that cluster near 4,341 ± 15 Myr, a single investigation has determined an age of 4.44 ± 0.05 Gyr for this sample (Nyquist et al. 1981).

The most reliable crystallization ages can be identified using some of the criteria outlined in the **Supplemental Text**. Doing so yields a preponderance of Mg-suite ages between 4.30 and 4.36 Gyr (**Supplemental Table 2**). The most robust age determinations are identified by concordance between multiple investigations and chronometric systems and are characterized by isochron regressions with the lowest uncertainties and MSWDs. The weighted average ages of the four Mg-suite rocks with the most tightly constrained ages are plotted on **Figure 9** along with a whole rock isochron age defined by Mg-suite rocks from Apollo 14, 15, 16, and 17 landing sites (see Borg et al. 2020). The ages determined in the most recent studies on 78236/8, 77215, 67667, and 15445 range from 4,331 to 4,364 Myr and are concordant with the Apollo 14, 15, 16, and 17 whole rock isochron age of 4,348 ± 25 Myr (Borg et al. 2020). In contrast, the average of six age determinations of 76535 is 4,304 ± 10 Myr (2 SD), which is about 50 Myr younger. However, 76535 is arguably the slowest cooled rock that has been successfully dated from the Moon, and the young age probably does not record crystallization. Instead, the 4.30 Gyr age reflects when

diffusion of Sm and Nd ceased in this sample as it cooled in the deep lunar crust or upper mantle (McCallum et al. 2006, Borg et al. 2017).

The observation that Mg-suite magmatism appears to have been contemporaneous at distant Apollo landing sites suggests that it was widespread over much of the lunar nearside between 4.30 to 4.36 Gyr. Furthermore, the ages of Mg-suite samples are not distinguishable from ages determined on LMO cumulates (**Figure 9**), suggesting a petrogenetic relationship between Mg-suite magmatism and LMO crystallization. The duration of Mg-suite magmatism is difficult to establish from the existing data. Although a few young ages have been reported for Mg-suite samples, none of these young ages have been duplicated in more recent studies. As a result, no unambiguous crystallization ages for Mg-suite rocks younger than 4.30 Gyr have been identified so far, suggesting Mg-suite magmatism represents a pulse of concentrated igneous activity that occurred at roughly the same time as the LMO crystallized.

Mg-suite magmatism has been proposed to originate in response to a stochastic event such as solidification of the LMO (Wood 1975, Longhi & Boudreau 1979, Raedeke & McCallum 1980), melting due to a large impact (Taylor et al. 1993, Hess 1994), or melting of the mantle as a result of overturn of the LMO (Shearer et al. 2015, Prissel et al. 2016, Borg et al. 2020, Prissel & Gross 2020, Zhang et al. 2021). Petrogenetic models for the origin of Mg-suite rocks indicate that they are derived from previously crystallized LMO sources including Mg-rich mafic cumulates, Ca-rich plagioclase, and urKREEP (e.g., Snyder et al. 1995a, Shervais & McGee 1999, Shearer et al. 2015). As a consequence, Mg-suite magmatism must postdate crystallization of the LMO. Production of the Mg-suite by heating and melting of the mantle by long-term processes, such as radioactive decay, is not consistent with the limited range of Mg-suite ages measured so far. Like the mare basalt sources, FAS, and urKREEP, the Mg-suite parental magmas appear to be derived from reservoirs with chondritic Sm-Nd isotope systematics [e.g., they have initial ε^{143}Nd near 0 (**Supplemental Table 2**)]. This is inconsistent with an origin by impact melting because the target protoliths would almost certainly be differentiated and have nonchondritic isotopic compositions at the time of impact. In addition, Mg-suite rocks have very low siderophile element abundances (Warren 1993), and most demonstrate evidence for slow cooling in the deep lunar interior (McCallum et al. 2006). Therefore, the temporal and geochemical characteristics of the Mg-suite appear to be most compatible with production by overturn of the LMO during, or soon after, its solidification. This scenario is appealing because it accounts for a pulse of magmatism that was derived from multiple LMO cumulate sources that were physically separated during initial crystallization of the LMO and mixed during the production of the parental Mg-suite melts. It is also consistent with recent rheologic modeling that suggests overturn is much more plausible just after or in the last stages of LMO solidification than it is later, after the LMO has cooled substantially (Yu et al. 2019).

4.2. Ages of the Alkali-Suite

Although both the Mg-suite and alkali-suite have high abundances of incompatible elements, indicative of the involvement of urKREEP in their petrogenesis, their geologic relationship is enigmatic. Some have argued these rock suites are derived from distinct parents with compositions similar to the parental melts of the Apollo 15 KREEP basalts (Snyder et al. 1995b). Others have suggested that they are more closely related, and that both Mg-suite and alkali-suite rocks are complementary cumulates of a common plutonic sequence (Shervais & McGee 1999). The chronology of the alkali-suite potentially offers some insights into this problem. If the two suites are closely related, then they should share the same range of ages; if they are unrelated, the range of crystallization ages could be distinct.

Only one attempt to date an alkali-suite rock has been made using the Sm-Nd and Rb-Sr chronometers, and it yielded vastly discordant ages of 4,108 ± 40 Myr and 4,324 ± 110 Myr (Snyder et al. 1995b). As a consequence, dating using the U-Pb chronometer of lunar zircons believed to derive from disaggregated alkali-suite rocks has provided the best constraints on the timing and duration of alkali-suite magmatism. A histogram of zircon ages is plotted in **Figure 9**. The vast majority of lunar zircon ages are determined on micrometer-sized spots by secondary ion mass spectrometry. As a result, the frequency distribution presented in **Figure 9** is a little misleading because numerous ages have been determined from individual zircons. For example, a single zircon from clast-rich impact melt breccia 72215 has yielded more than 40 individual ages and represents more than 10% of the data plotted in **Figure 9**. The majority of zircons that have been dated are found in soils and lithic breccias where they have been separated from their host rocks and concentrated by intense impact processing. Transient heating associated with impact metamorphism has the potential to produce zircon overgrowths and mobilize Pb within individual zircon grains on the scale of ion microprobe spots, disturbing the original isotopic systematics of the zircons and resulting in ages that do not record crystallization (e.g., Pidgeon et al. 2007, Zhang et al. 2012, Grange et al. 2013, Cavosie et al. 2015).

Despite these limitations, there is clearly a peak of zircon ages at ∼4,340 ± 20 Myr (Borg et al. 2015) (**Figure 9**) that coincides with the ages of both the LMO cumulates and the Mg-suite samples. In addition, the oldest zircon age determined by the more precise isotope dilution thermal ionization mass spectrometry method is 4,335 ± 3 Myr (Barboni et al. 2017). This suggests that a significant volume of alkali-suite magma was produced contemporaneously with Mg-suite magmatism and LMO cumulate formation. However, unlike Mg-suite magmatism, the zircon ages from alkali-suite magmas demonstrate a significant range, terminating around the time of the Imbrium impact at ∼3.8 Gyr. If some of these younger ages record primary igneous activity, then the alkali-suite is not likely to be related to the Mg-suite as suggested by Snyder et al. (1995b) and instead is probably associated with KREEP basaltic magmatism that extends to at least ∼3.0 Gyr (Borg et al. 2004, Nemchin et al. 2008).

5. CONCLUSION

Isotopic measurements have been made on a variety of lunar and terrestrial materials with the goal of determining when the Moon formed. The conclusions of these investigations often contradict one another, making a simple interpretation of the earliest events in the history of the Earth-Moon system difficult to discern. The contradictory nature of much of the chronology stems from a variety of factors including disturbance of ages by secondary processes, calculation of model ages based on Myriad assumptions, erroneous measurements, and an ever-evolving understanding of the petrogenesis of the dated samples. The result is that seemingly legitimate ages for the Moon have been proposed that span more than 200 Myr.

Figure 10 provides a summary of the key events in lunar evolution along with the best current constraints on their timing. Key events include volatile element depletion of the protoplanetary disk, the giant impact, crystallization of the LMO, emplacement of the Mg-suite that potentially marks the onset of mantle overturn, and emplacement of the alkali-suite. Although dating approaches sensitive to when the Moon became depleted in volatile elements point to formation of the Moon within a couple of million years of the Solar System (4,566 to 4,561 Myr), these ages likely reflect the formation of the materials from which the Moon was made, not necessarily when the Moon itself formed. Similarly, Hf-W data for the Moon cannot distinguish between events that occurred on the Moon and those that occurred on the bodies from which the Moon formed. The one process that provides a firm constraint on the formation age of the Moon is

crystallization of the LMO. Crystallization of the LMO produced a variety of cumulate lithologies that can be dated including the mafic cumulate source of the mare basalts, the flotation cumulates of the FAS, and late-stage incompatible element-enriched residue of the LMO known as urKREEP. The most rigorous time constraint that can be derived from the Hf-W isotopic system is based on the observation that the products of the LMO have quite distinct Hf/W ratios but similar $^{182}W/^{184}W$. This result indicates that they formed after the extinction of ^{182}Hf, pushing the age of the LMO to less than 4.50 Gyr. The ages derived from LMO crystallization products range from 4,336 to 4,361 Myr. The small range of ages measured between early and late-stage crystallization products of the LMO suggest it crystallized over a few tens of millions of years at most. The Mg-suite is intruded into the primordial FAS crust and therefore provides a minimum age of LMO solidification of 4,364 Myr. This suite of rocks has been suggested to have been produced by overturn of the LMO, in which case overturn must have occurred contemporaneously with, or immediately following, LMO crystallization. The alkali-suite is another post-LMO crustal rock type that has been dated using detrital zircons found in soils and breccias. The peak of zircon ages around 4,340 Myr indicates that this suite is contemporaneous with the Mg-suite. Although zircon ages as young as ~3.8 Gyr have been observed, they may record the Imbrium impact event rather than emplacement of late alkali-suite magmas into the crust. As the record of mare basalt volcanism now extends to 2 Gyr (Che et al. 2021, Li et al. 2021), lunar magmatism clearly did not end following LMO crystallization. In total the chronology depicts a concentrated period of geologic activity on the Moon in which the LMO crystallized and a secondary crust, represented by the Mg-suite and alkali-suite, was produced over a relatively short time interval of a few tens of millions of years about 4.36 Gyr.

The question that remains is how close this unexpectedly young age comes to the time of Moon formation. No physical model that we are aware of provides a mechanism that would keep the Moon in a largely molten state for 150–200 Myr prior to the initiation of LMO crystallization or preserve an already-formed Moon in Earth's orbit that was hit hard enough to cause a global magma ocean 150–200 Myr after Moon formation. Models for planetary accumulation provide no strong upper limit on the time between the start of planet formation and the last major impact between planetary embryos and hence do not rule out a late Moon-forming impact into the proto-Earth. Given the small and restricted region from which the available lunar samples derive, the possibility exists that the samples were not derived from a global magma ocean but instead represent the crystallization products of a large magma lake formed by a huge impact into an already-formed Moon. Given the preponderance of anorthositic crust on the Moon, and the great depth of origin of mare basalts, this explanation seems unlikely, however. An argument in favor of late Moon formation is that a variety of avenues to determine the age of the oldest silicate differentiation events on Earth provide ages overlapping those of LMO crystallization (Carlson et al. 2015, Connelly & Bizzarro 2016). The chronologic complications discussed in this review and in the **Supplemental Text** for determining the time of Moon formation are much more severe for Earth, as it has remained geologically active throughout its history, resulting in only a few parts per million of its surface area preserving rocks older than 3.5 Gyr. As a result, none of the age data relevant to Earth formation provide a precise age for the Moon-forming impact. We suggest that the ~4.36 Gyr ages defined by LMO cumulates provide our most precise information on the timing of the giant impact and the formation of the Moon.

DISCLOSURE STATEMENT

The authors are not aware of any affiliations, memberships, funding, or financial holdings that might be perceived as affecting the objectivity of this review.

ACKNOWLEDGMENTS

This work was performed under the auspices of the US Department of Energy by the Lawrence Livermore National Laboratory under contract DE-AC52-07NA27344, with release number LLNL-JRNL-830769. This work was supported by Laboratory Directed Research and Development grant 20-ERD-001 and NASA Emerging Worlds Program grant NNH16AC441 (L.E.B.). R.W.C. thanks the Carnegie Institution for Science for support. Finally, we would like to acknowledge the contribution of the pioneers of lunar chronology, William Compston, Gunter Lugmair, Larry Nyquist, Mitsunobu Tatsumoto, George Tilton, and Gerald Wasserburg, and their many colleagues whose work started us down the same path.

LITERATURE CITED

Alibert C, Norman MD, McCulloch MT. 1994. An ancient Sm-Nd age for a ferroan noritic anorthosite clast from lunar breccia 67016. *Geochim. Cosmochim. Acta* 58:2921–26

Amelin Y, Krot AN, Hutcheon ID, Ulyanov AA. 2002. Lead isotopic ages of chondrules and calcium-aluminum-rich inclusions. *Science* 297:1678–83

Barboni M, Boehnke P, Keller B, Kohl IE, Schoene B, et al. 2017. Early formation of the Moon 4.51 billion years ago. *Sci. Adv.* 3:e1602365

Bonnand P, Williams HM, Parkinson IJ, Wood BJ, Halliday AN. 2016. Stable chromium isotopic composition of meteorites and metal-silicate experiments: implications for fractionation during core formation. *Earth Planet. Sci. Lett.* 435:14–21

Borg LE, Brennecka GA, Kruijer TS. 2022. The origin of volatile elements in the Earth–Moon system. *PNAS* 119:e2115726119

Borg LE, Brennecka GA, Symes SJ. 2016. Accretion timescale and impact history of Mars deduced from the isotopic systematics of martian meteorites. *Geochim. Cosmochim. Acta* 175:150–67

Borg LE, Cassata WS, Wimpenny J, Gaffney AM, Shearer CK. 2020. The formation and evolution of the Moon's crust inferred from the Sm-Nd isotopic systematics of highlands rocks. *Geochim. Cosmochim. Acta* 290:312–32

Borg LE, Connelly JN, Boyet M, Carlson RW. 2011. Chronological evidence that the Moon is either young or did not have a global magma ocean. *Nature* 477:70–72

Borg LE, Connelly JN, Cassata WS, Gaffney AM, Bizzarro M. 2017. Chronologic implications for slow cooling of troctolite 76535 and temporal relationships between the Mg-suite and the ferroan anorthosite suite. *Geochim. Cosmochim. Acta* 201:377–91

Borg LE, Gaffney AM, Kruijer TS, Marks NA, Sio CK, Wimpenny J. 2019. Isotopic evidence for a young lunar magma ocean. *Earth Planet. Sci. Lett.* 523:115706

Borg LE, Gaffney AM, Shearer CK. 2015. A review of lunar chronology revealing a preponderance of 4.34–4.37 Ga ages. *Meteorit. Planet. Sci.* 50:715–32

Borg LE, Norman M, Nyquist L, Bogard D, Snyder G, et al. 1999. Isotopic studies of ferroan anorthosite 62236: a young lunar crustal rock from a light rare-earth-element-depleted source. *Geochim. Cosmochim. Acta* 63:2679–91

Borg LE, Nyquist LE, Taylor LA, Wiesmann H, Shih CY. 1997. Constraints on Martian differentiation processes from Rb-Sr and Sm-Nd isotopic analyses of the basaltic shergottite QUE 94201. *Geochim. Cosmochim. Acta* 61:4915–31

Borg LE, Shearer CK, Asmerom Y, Papike JJ. 2004. Prolonged KREEP magmatism on the Moon indicated by the youngest dated lunar igneous rock. *Nature* 432:209–11

Bouvier A, Vervoort JD, Patchett PJ. 2008. The Lu–Hf and Sm–Nd isotopic composition of CHUR: constraints from unequilibrated chondrites and implications for the bulk composition of terrestrial planets. *Earth Planet. Sci. Lett.* 273:48–57

Boyet M, Carlson RW. 2007. A highly depleted moon or a non-magma ocean origin for the lunar crust? *Earth Planet. Sci. Lett.* 262:505–16

Boyet M, Carlson RW, Borg LE, Horan M. 2015. Sm–Nd systematics of lunar ferroan anorthositic suite rocks: constraints on lunar crust formation. *Geochim. Cosmochim. Acta* 148:203–18

Brandon AD, Lapen TJ, Debaille V, Beard BL, Rankenburg K, Neal C. 2009. Re-evaluating $^{142}Nd/^{144}Nd$ in lunar mare basalts with implications for the early evolution and bulk Sm/Nd of the Moon. *Geochim. Cosmochim. Acta* 73:6421–45

Brown GM, Emeleus CH, Holland JG. Peckett A, Phillips R. 1972. Mineral-chemical variations in Apollo 14 and Apollo 15 basalts and granitic fractions. *Proc. Lunar Planet. Sci. Conf.* 3:141–57

Burkhardt C, Borg LE, Brennecka GA, Shollenberger QR, Dauphas N, Kleine T. 2016. A nucleosynthetic origin for the Earth's anomalous ^{142}Nd composition. *Nature* 537:394–98

Carlson RW, Borg LE, Gaffney AM, Boyet M. 2014. Rb-Sr, Sm-Nd and Lu-Hf isotope systematics of the lunar Mg-suite: the age of the lunar crust and its relation to the time of Moon formation. *Philos. Trans. R. Soc. A* 372(2024):20130246

Carlson RW, Boyet M, O'Neil J, Rizo H, Walker RJ. 2015. Early differentiation and its long-term consequences for Earth evolution. In *The Early Earth: Accretion and Differentiation*, ed. J Badro, M Walter, pp. 143–72. Washington, DC: Am. Geophys. Union

Carlson RW, Lugmair GW. 1979. Sm–Nd constraints on early lunar differentiation and the evolution of KREEP. *Earth Planet. Sci. Lett.* 45:123–32

Carlson RW, Lugmair GW. 1981. Time and duration of lunar highlands crust formation. *Earth Planet. Sci. Lett.* 52:227–38

Carlson RW, Lugmair GW. 1988. The age of ferroan anorthosite 60025: oldest crust on a young Moon? *Earth Planet. Sci. Lett.* 90:119–30

Cavosie AJ, Erickson TM, Timms NE, Reddy SM, Talavera C, et al. 2015. A terrestrial perspective on using ex situ shocked zircons to date lunar impacts. *Geology* 43:999–1002

Chambers JE. 2004. Planetary accretion in the inner Solar System. *Earth Planet. Sci. Lett.* 223:241–52

Che X, Nemchin A, Liu D, Long T, Wang C, et al. 2021. Age and composition of young basalts on the Moon, measured from samples returned by Chang'e-5. *Science* 374:887–90

Compston W, Berry H, Vernon MJ, Chappell BW, Kaye MJ. 1971. Rubidium-strontium chronology and chemistry of lunar material from the Ocean of Storms. *Proc. Lunar Planet. Sci. Conf.* 2:1471–85

Connelly JN, Bizzarro M. 2016. Lead isotope evidence for a young formation age of the Earth–Moon system. *Earth Planet. Sci. Lett.* 452:36–43

Connelly JN, Bizzarro M, Krot AN, Nordlund A, Wielandt D, Ivanova MA. 2012. The absolute chronology and thermal processing of solids in the Solar protoplanetary disk. *Science* 338:651–55

Edmunson J, Borg LE, Nyquist LE, Asmerom Y. 2009. A combined Sm–Nd, Rb–Sr, and U–Pb isotopic study of Mg-suite norite 78238: further evidence for early differentiation of the Moon. *Geochim. Cosmochim. Acta* 73:514–27

Elardo SM, Draper DS, Shearer CK. 2011. Lunar magma ocean crystallization revisited: bulk composition, early cumulate mineralogy, and the source regions of the highlands Mg-suite. *Geochim. Cosmochim. Acta* 75:3024–45

Elkins-Tanton LT, Burgess S, Yin QZ. 2011. The lunar magma ocean: reconciling the solidification process with lunar petrology and geochronology. *Earth Planet. Sci. Lett.* 304:326–36

Elkins-Tanton LT, Van Orman JA, Hager BH, Grove TL. 2002. Re-examination of the lunar magma ocean cumulate overturn hypothesis: Melting or mixing is required. *Earth Planet. Sci. Lett.* 196:239–49

Gaffney AM, Borg LE. 2014. A young solidification age for the lunar magma ocean. *Geochim. Cosmochim. Acta* 140:227–40

Gaffney AM, Borg LE, Shearer CK, Burger PV. 2015. Chronology of 15445 Norite clast B and implication for Mg-suite magmatism. *Proc. Lunar Planet. Sci. Conf.* 2015:1443 (Abstr.)

Grange ML, Nemchim AA, Pidgeon RT, Muhling JR, Kennedy AK. 2009. Thermal history recorded by the Apollo 17 impact melt breccia 73217. *Geochim. Cosmochim. Acta* 73:3093–107

Grange ML, Nemchin AA, Timms N, Pidgeon RT, Meyer C. 2011. Complex magmatic and impact history prior to 4.1 Ga recorded in zircon from Apollo 17 South Massif aphanitic breccia 73235. *Geochim. Cosmochim. Acta* 75:2213–32

Grange ML, Pidgeon RT, Nemchin AA, Timms NE, Meyer C. 2013. Interpreting U–Pb data from primary and secondary features in lunar zircon. *Geochim. Cosmochim. Acta* 101:112–32

Halliday AN, Porcelli D. 2001. In search of lost planets—the paleocosmochemistry of the inner solar system. *Earth Planet. Sci. Lett.* 192:545–59

Hanan BB, Tilton GR. 1987. 60025: Relict of primitive lunar crust? *Earth Planet. Sci. Lett.* 84:15–21
Hans U, Kleine T, Bourdon B. 2013. Rb–Sr chronology of volatile depletion in differentiated protoplanets: BABI, ADOR and ALL revisited. *Earth Planet. Sci. Lett.* 374:204–14
Hartmann WK, Davis DR. 1975. Satellite-sized planetesimals and lunar origin. *Icarus* 24:504–15
Hess PC. 1994. The petrogenesis of lunar troctolites. *J. Geophys. Res.* 99(E9):19083–93
Jahn B-M, Gruau G, Glickson AY. 1982. Komatiites of the Onverwacht Group, S. Africa: REE geochemistry, Sm/Nd age and mantle evolution. *Contrib. Minerol. Petrol.* 80:25–40
James OB. 1980. Rocks of the early lunar crust. *Proc. Lunar Planet. Sci. Conf.* 11:365–93
Keays RR, Ganapathy R, Laul JC, Anders E, Herzog GF, Jeffery PM. 1970. Trace elements and radioactivity in lunar rocks: implications for meteorite infall, solar-wind flux and formation conditions of Moon. *Science* 167:490–93
Kinoshita N, Paul M, Kashiv Y, Collon P, Deibel CM, et al. 2012. A shorter ^{146}Sm half-life measured and implications for ^{146}Sm-^{142}Nd chronology in the solar system. *Science* 335:1614–17
Kleine T, Palme H, Mezger K, Halliday AN. 2005. Hf-W chronometry of lunar metals and the age and early differentiation of the Moon. *Science* 310:1671–74
Kruijer TS, Archer GJ, Kleine T. 2021. No ^{182}W evidence for early Moon formation. *Nat. Geosci.* 14:714–15
Kruijer TS, Kleine T. 2017. Tungsten isotopes and the origin of the Moon. *Earth Planet. Sci. Lett.* 475:15–24
Kruijer TS, Kleine T, Fischer-Godde M, Sprung P. 2015. Lunar tungsten isotopic evidence for the late veneer. *Nature* 520:534–37
Laneuville M, Wieczorek MA, Breuer D, Tosi N. 2013. Asymmetric thermal evolution of the Moon. *J. Geophys. Res. Planets* 118:1435–52
Lee D-C, Halliday AN, Leya I, Wieler R, Wiechert U. 2002. Cosmogenic tungsten and the origin and earliest differentiation of the Moon. *Earth Planet. Sci. Lett.* 198:267–74
Lee D-C, Halliday AN, Snyder GA, Taylor LA. 1997. Age and origin of the Moon. *Science* 278:1098–103
Levison HF, Kretke KA, Walsh KJ, Bottke WF. 2015. Growing the terrestrial planets from the gradual accumulation of submeter-sized objects. *PNAS* 112:14180–85
Leya I, Wieler R, Halliday AN. 2000. Cosmic-ray production of tungsten isotopes in lunar samples and meteorites and its implications for Hf–W cosmochemistry. *Earth Planet. Sci. Lett.* 175:1–12
Li QL, Zhou Q, Liu Y, Xiao Z, Lin Y, et al. 2021. Two-billion-year-old volcanism on the Moon from Chang'e-5 basalts. *Nature* 600:54–58
Lin Y, Tronche EJ, Steenstra ES, van Westrenen W. 2017. Experimental constraints on the solidification of a nominally dry lunar magma ocean. *Earth Planet. Sci. Lett.* 471:104–16
Longhi J. 1977. Magma oceanography 2: chemical evolution and crustal formation. *Proc. Lunar Planet. Sci. Conf.* 8:601–21
Longhi J, Boudreau AE. 1979. Complex igneous processes and the formation of the primitive lunar crustal rocks. *Proc. Lunar Planet. Sci. Conf.* 10:2085–105
Lugmair GW, Carlson RW. 1978. The Sm-Nd history of KREEP. *Proc. Lunar Planet. Sci. Conf.* 9:689–704
Lugmair GW, Marti K, Kurtz JP, Scheinin NB. 1976. History and genesis of lunar troctolite 76535 or: How old is old? Proc. *Proc. Lunar Planet. Sci. Conf.* 7:2009–33
Lugmair GW, Shukolyukov A. 1998. Early solar system timescales according to ^{53}Mn-^{53}Cr systematics. *Geochim. Cosmochim. Acta* 62:2863–86
Markowski A, Quitte G, Kleine T, Halliday A, Bizzarro M, Irving A. 2007. Hafnium–tungsten chronometry of angrites and the earliest evolution of planetary objects. *Earth Planet. Sci. Lett.* 262:214–29
Marks NE, Borg LE, Hutcheon ID, Jacobsen B, Clayton RN. 2014. Samarium–neodymium chronology and rubidium–strontium systematics of an Allende calcium–aluminum-rich inclusion with implications for ^{146}Sm half-life. *Earth Planet. Sci. Lett.* 405:15–24
Marks NE, Borg LE, Shearer CK, Cassata WS. 2019. Geochronology of an Apollo 16 clast provides evidence for a basin-forming impact 4.3 billion years ago. *J. Geophys. Res. Planets* 124:2465–81
Maurice M, Tosi N, Schwinger S, Breuer D, Kleine T. 2020. A long-lived magma ocean on a young Moon. *Sci. Adv.* 6:eaba8949
McCallum IS, Domeneghetti MC, Schwartz JM, Mullen EK, Zema M, et al. 2006. Cooling history of lunar Mg-suite gabbronorite 76255, troctolite 76535 and Stillwater pyroxenite SC-936: the record in exsolution and ordering in pyroxenes. *Geochim. Cosmochim. Acta* 70:6068–78

McDonough WF, Sun S-S. 1995. The composition of the Earth. *Chem. Geol.* 120:223–53
McLeod CL, Brandon AD, Armytage RMG. 2014. Constraints on the formation age and evolution of the Moon from ^{142}Nd–^{143}Nd systematics of Apollo 12 basalts. *Earth Planet. Sci. Lett.* 396:179–89
Meissner F, Schmidt-Ott WD, Ziegeler L. 1987. Half-life and α-ray energy of ^{146}Sm. *Z. Phys. A Atom. Nuclei* 327:171–74
Meyer C, Williams IS, Compston W. 1996. Uranium-lead ages for lunar zircons: evidence for a prolonged period of granophyre formation from 4.32 to 3.88 Ga. *Meteorit. Planet. Sci.* 31:370–87
Morrison GH, Gerard JT, Kashuba AT, Gangadharam EV, Rothenburg AM, et al. 1970. Multielement analysis of lunar soils and rocks. *Science* 167:505–7
Nemchin A, Timms N, Pidgeon R, Geisler T, Reddy S, Meyer C. 2009a. Timing of crystallization of the lunar magma ocean constrained by the oldest zircon. *Nat. Geosci.* 2:133–36
Nemchin AA, Pidgeon RT, Healy D, Grange ML, Whithouse MJ, Vaughan J. 2009b. The comparative behavior of apatite-zircon U-Pb systems in Apollo 14 breccias: implications for the thermal history of the Fra Mauro Formation. *Meteorit. Planet. Sci.* 44:1717–34
Nemchin AA, Pidgeon RT, Whitehouse MJ, Vaughan JP, Meyer C. 2008. SIMS U–Pb study of zircon from Apollo 14 and 17 breccias: implications for the evolution of lunar KREEP. *Geochim. Cosmochim. Acta* 72:668–89
Nemchin AA, Whitehouse MJ, Pidgeon RT, Meyer C. 2006. Oxygen isotopic signature of 4.4–3.9 Ga zircons as a monitor of differentiation processes on the Moon. *Geochim. Cosmochim. Acta* 70:1864–72
Newsom HE. 1995. Composition of the solar system, planets, meteorites, and major terrestrial reservoirs. In *Global Earth Physics: A Handbook of Physical Constants*, ed. TJ Ahrens, pp. 159–89. Washington, DC: Am. Geophys. Union
Norman MD, Borg LE, Nyquist LE, Bogard DD. 2003. Chronology, geochemistry, and petrology of a ferroan noritic anorthosite clast from Descartes breccia 67215: clues to the age, origin, structure, and impact history of the lunar crust. *Meteorit. Planet. Sci.* 38:645–61
Nyquist LE, Bansal BM, Wiesmann H, Jahn B-M. 1974. Taurus-Littrow chronology: some constraints on early lunar crustal development. *Proc. Lunar Planet. Sci. Conf.* 5:1515–39
Nyquist LE, Bogard DD, Shih CY. 2001. Radiometric chronology of the Moon and Mars. In *The Century of Space Science*, ed. J Bleeker, J Geiss, M Huber, pp. 1325–76. Dordrecht, Neth.: Kluwer
Nyquist LE, Bogard DD, Yamaguchi A, Shih CY, Karouji Y, et al. 2006. Feldspathic clasts in Yamato-86032: remnants of the lunar crust with implications for its formation and impact history. *Geochim. Cosmochim. Acta* 70:5990–6015
Nyquist LE, Reimold WU, Bogard DD, Wooden JL, Bansal BM, et al. 1981. A comparative Rb–Sr, Sm–Nd, and K–Ar study of shocked norite 78236: evidence of slow cooling in the lunar crust? *Proc. Lunar Planet. Sci. Conf.* 12:67–97
Nyquist LE, Shih CY. 1992. The isotopic record of lunar volcanism. *Geochim. Cosmochim. Acta* 56:2213–34
Nyquist LE, Wiesmann H, Bansal B, Shih C-Y, Keith JE, Harper CL. 1995. ^{146}Sm-^{142}Nd formation interval for the lunar mantle. *Geochim. Cosmochim. Acta* 59:2817–37
Nunes PD, Tatsumoto M, Knight RJ, Unruh DM, Doe BR. 1973. U-Th-Pb systematics of some Apollo 16 lunar samples. *Proc. Lunar Planet. Sci. Conf.* 4:1797–822
Palme H. 1977. On the age of KREEP. *Geochim. Cosmochim. Acta* 41:1791–801
Palme H, O'Neill HSC. 2014. Cosmochemical estimates of mantle composition. In *Treatise on Geochemistry*, ed. RW Carlson, pp. 1–39. Amsterdam: Elsevier
Papanastassiou DA, Wasserburg GJ, Burnett DS. 1970. Rb-Sr ages of lunar rocks from the Sea of Tranquility. *Earth Planet. Sci. Lett.* 8:1–19
Papike JJ, Ryder G, Shearer CK. 2018. Lunar samples. In *Planetary Materials*, ed. JJ Papike, pp. 719–952. Boston: De Gruyter
Parmentier EM, Zhong S, Zuber MT. 2002. Gravitational differentiation due to initial chemical stratification: origin of lunar asymmetry by the creep of dense KREEP? *Earth Planet. Sci. Lett.* 201:473–80
Perera V, Jackson AP, Elkins-Tanton LT, Asphaug E. 2018. Effect of reimpacting debris on the solidification of the lunar magma ocean. *J. Geophys. Res. Planets* 123:1168–91
Pidgeon RT, Nemchin AA, Van Bronswijk W, Geisler T, Meyer C, et al. 2007. Complex history of a zircon aggregate from lunar breccia 73235. *Geochim. Cosmochim. Acta* 71:1370–81

Premo WR, Tatsumoto M, Wang JW. 1989. Pb isotopes in anorthositic breccias 67075 and 62237: a search for primitive lunar lead. *Proc. Lunar Planet. Sci. Conf.* 19:61–71

Prissel TC, Gross J. 2020. On the petrogenesis of lunar troctolites: new insights into cumulate mantle overturn and mantle exposures in impact basins. *Earth Planet. Sci. Lett.* 551:116531

Prissel TC, Parman SW, Head JW. 2016. Formation of the lunar highlands Mg-suite as told by spinel. *Am. Mineral.* 101:1624–35

Qin L, Alexander CMOD, Carlson RW, Horan MF, Yokoyama T. 2010. Contributors to chromium isotope variation in meteorites. *Geochim. Cosmochim. Acta* 74:1122–45

Quillen AC, Martini L, Nakajima M. 2019. Near/far side asymmetry in the tidally heated Moon. *Icarus* 329:182–96

Raedeke LD, McCallum IS. 1980. A comparison of the fractionation trends in the lunar crust and the Stillwater Complex. In *Proceedings of the Conference on the Lunar Highlands Crust*, pp. 133–53. New York: Pergamon Press

Rankenburg K, Brandon AD, Neal CR. 2006. Neodymium isotope evidence for a chondritic composition of the Moon. *Science* 312:1369–72

Rapp JF, Draper DS. 2018. Fractional crystallization of the lunar magma ocean: updating the dominant paradigm. *Meteorit. Planet. Sci.* 53:1432–55

Ringwood AE, Kesson SE. 1976. A dynamic model for mare basalt petrogenesis. *Proc. Lunar Planet. Sci. Conf.* 7:1697–722

Sedaghatpour F, Teng FZ, Liu Y, Sears DW, Taylor LA. 2013. Magnesium isotopic composition of the Moon. *Geochim. Cosmochim. Acta* 120:1–16

Shearer CK, Elardo SM, Petro NE, Borg LE, McCubbin FM. 2015. Origin of the lunar highlands Mg-suite: an integrated petrology, geochemistry, chronology, and remote sensing perspective. *Am. Minerol.* 100:294–325

Shearer CK, Hess PC, Wieczorek MA, Pritchard ME, Parmentier EM, et al. 2006. Thermal and magmatic evolution of the Moon. *Rev. Mineral. Geochem.* 60:365–518

Shervais JW, McGee JJ. 1999. KREEP cumulates in the western lunar highlands: ion and electron microprobe study of alkali-suite anorthosites and norites from Apollo 12 and 14. *Am. Minerol.* 84:806–20

Shih CY, Nyquist LE, Dasch EJ, Bogard DD, Bansal BM, Wiesmann H. 1993. Ages of pristine noritic clasts from lunar breccias 15445 and 15455. *Geochim. Cosmochim. Acta* 57:915–31

Sio CK, Borg LE, Cassata WS. 2020. The timing of lunar solidification and mantle overturn recorded in ferroan anorthosite 62237. *Earth Planet. Sci. Lett.* 538:116219

Smith JV, Anderson AT, Newton RC, Olsen EJ, Wyllie PJ. 1970. Petrologic history of the Moon inferred from petrography, mineralogy, and petrogenesis of Apollo 11 rocks. *Goechim. Cosmochim. Acta* 11(Supp.):897–925

Snape JF, Nemchin AA, Bellucci JJ, Whitehouse MJ, Tartese R, et al. 2016. Lunar basalt chronology, mantle differentiation and implications for determining the age of the Moon. *Earth Planet. Sci. Lett.* 451:149–58

Snyder GA, Borg LE, Nyquist LE, Taylor LA. 2000. Chronology and isotopic constraints on lunar evolution. In *Origin of the Earth and Moon*, ed. R Canup, K Righter, pp. 361–95. Tucson: University of Arizona Press

Snyder GA, Neal CR, Taylor LA, Halliday AN. 1995a. Processes involved in the formation of the magnesian-suite plutonic rocks from the highlands of the Earth's Moon. *J. Geophys. Res.* 100(E5):9365–88

Snyder GA, Taylor LA, Jerde EA, Halliday AN. 1995b. Chronology and petrogenesis of the lunar highlands alkali suite: cumulates of KREEP basalt crystallization. *Geochim. Cosmochim. Acta* 59:1185–203

Snyder GA, Taylor LA, Neal CR. 1992. A chemical model for generating the sources of mare basalts: combined equilibrium and fractional crystallization of the lunar magmasphere. *Geochim. Cosmochim. Acta* 56:3809–23

Solomon SC, Longhi J. 1977. Magma oceanography: 1. Thermal evolution. *Proc. Lunar Planet. Sci. Conf.* 8:583–99

Sprung P, Kleine T, Scherer EE. 2013. Isotopic evidence for chondritic Lu/Hf and Sm/Nd of the Moon. *Earth Planet. Sci. Lett.* 380:77–87

Stacey JS, Kramers JD. 1975. Approximation of terrestrial lead isotope evolution by a two-stage model. *Earth Planet. Sci. Lett.* 26:207–21

Taylor DJ, McKeegan KD, Harrison TM. 2009. Lu–Hf zircon evidence for rapid lunar differentiation. *Earth Planet. Sci. Lett.* 279:157–64

Taylor SR, Norman MD. 1990. Accretion of differentiated planetesimals to the Earth. In *Origin Earth*, pp. 29–43. Houston, TX: Lunar Planet. Inst.

Taylor SR, Norman MD, Esat TM. 1993. The Mg-suite and the highland crust: an unsolved enigma. *Proc. Lunar Planet. Sci. Conf.* 24:1413–14 (Abstr.)

Tera F, Papanastassiou DA, Wasserburg GJ. 1974. Isotopic evidence for a terminal lunar cataclysm. *Earth Planet. Sci. Lett.* 22:1–21

Tera F, Wasserburg GJ. 1972. U-Th-Pb systematics in lunar highland samples from the Luna 20 and Apollo 16 missions. *Earth Planet. Sci. Lett.* 17:36–51

Tera F, Wasserburg GJ. 1974. U-Th-Pb systematics on lunar rocks and inferences about lunar evolution and the age of the moon. *Proc. Lunar Planet. Sci. Conf.* 5:1571–99

Thiemens MM, Sprung P, Fonseca ROC, Leitzke FP, Munker C. 2019. Early Moon formation inferred from hafnium–tungsten systematics. *Nat. Geosci.* 12:696–700

Touboul M, Kleine T, Bourdon B, Palme H, Wieler R. 2007. Late formation and prolonged differentiation of the Moon inferred from W isotopes in lunar metals. *Nature* 450:1206–9

Touboul M, Kleine T, Bourdon B, Palme H, Wieler R. 2009. Tungsten isotopes in ferroan anorthosites: implications for the age of the Moon and lifetime of its magma ocean. *Icarus* 199:245–49

Touboul M, Puchtel IS, Walker RJ. 2015. Tungsten isotopic evidence for disproportional late accretion to the Earth and Moon. *Nature* 520:530–33

Urey HC. 1951. The origin and development of the earth and other terrestrial planets. *Geochim. Cosmochim. Acta* 1:209–77

Walker D, Longhi J, Hays JF. 1975. Differentiation of a very thick magma body and implications for the source regions of mare basalts. *Proc. Lunar Planet. Sci. Conf.* 6:1103–20

Warren PH. 1985. The magma ocean concept and lunar evolution. *Annu. Rev. Earth Planet. Sci.* 13:201–40

Warren PH. 1989. KREEP: major-element diversity, trace-element uniformity (almost). In *Moon in Transition: Apollo 14, KREEP, and Evolved Lunar Rocks*, pp. 149–53. Houston, TX: Lunar Planet. Inst.

Warren PH. 1993. A concise compilation of petrologic information on possibly pristine nonmare Moon rocks. *Am. Minerol.* 78:360–76

Warren PH, Wasson JT. 1979. The origin of KREEP. *Rev. Geophys.* 17:73–88

Warren PH, Wasson JT. 1980. Further foraging for pristine nonmare rocks: correlations between geochemistry and longitude. *Proc. Lunar Planet. Sci. Conf.* 11:431–70

Wieczorek MA, Phillips RJ. 2000. The "Procellarum KREEP Terrane": implications for mare volcanism and lunar evolution. *J. Geophys. Res. Planets* 105:20417–30

Wood JA. 1975. Lunar petrogenesis in a well-stirred magma ocean. *Proc. Lunar Planet. Sci. Conf.* 6:1087–102

Wood JA, Dickey JS Jr., Marvin UB, Powell BN. 1970. Lunar anorthosites and a geophysical model of the moon. *Geochim. Cosmochim. Acta* 11(Supp.):965–88

Yu S, Tosi N, Schwinger S, Maurice M, Breuer D, Xiao L. 2019. Overturn of ilmenite-bearing cumulates in a rheologically weak lunar mantle. *J. Geophys. Res. Planets* 124:418–36

Zhang A-C, Taylor LA, Wang R-C, Li Q-L, Li X-H, et al. 2012. Thermal history of Apollo 12 granite and KREEP-rich rock: clues from Pb/Pb ages of zircon in lunar breccia 12013. *Geochim. Cosmochim. Acta* 95:1–14

Zhang B, Lin Y, Moser DE, Warren PH, Hao J, et al. 2021. Timing of lunar Mg-suite magmatism constrained by SIMS U-Pb dating of Apollo norite 78238. *Earth Planet. Sci. Lett.* 569:117046

Supplemental Material: Annu. Rev. Earth. Planet. Sci. 2023. 51:25-52
https://doi.org/10.1146/annurev-earth-031621-060538

SUPPLEMENTAL TEXT

The Evolving Chronology of Moon Formation

Lars E. Borg[1]

Richard W. Carlson[2]

1. Nuclear and Chemical Science Division, Lawrence Livermore National Laboratory, 7000 East Avenue L-231 Livermore CA 94550 USA

2. Earth and Planets Laboratory, Carnegie Institution for Science, 5241 Broad Branch Road, NW Washington, DC 20015-1305 USA

1. INTRODUCTION

The goal of this supplement is to describe the most important challenges associated with geochronologic measurements completed on lunar samples. Whereas determining ages of young basaltic rocks from the Moon is relatively straightforward, dating lunar magma ocean cumulates is often quite challenging. These challenges arise because the Moon's surface is a unique neutron-rich environment dominated by thermal metamorphism associated with numerous large impact events onto targets comprised of unusual rock types. Therefore, chronologic measurements completed on samples from other planetary bodies do not always serve as good proxies for dating the most ancient events in lunar history. This supplement is essentially a compilation of our experiences (difficulties, pitfalls, and lessons learned) gained from years of work completing chronologic measurements on lunar samples. The hope is that it will serve as both a resource for future lunar chronologic investigations and as an explanation for the current confused state of lunar chronology. Below we discuss: (1) the strengths and weaknesses of radiometric approaches to determining the age of the Moon, (2) the factors affecting Rb-Sr, Sm-Nd, Lu-Hf isochron ages, (3) the application of the U-Pb system to lunar chronology, and (4) model age systematics associated with both individual samples and suites of samples.

2. STRENGTHS AND WEAKNESSES OF RADIOMETRIC APPROACHES TO DETERMINING THE AGE OF THE MOON

Essentially the only way to obtain absolute ages of useful precision for lunar differentiation is through the application of various radioactive chronometers to rock and mineral samples from the Moon. Under the best of circumstances, modern radioactive dating techniques can achieve age precisions in the 10^5 year range for samples as old as four and a half billion years (e.g., Connelly et al 2017). These chronometers date events that fractionate the radioactive parent from the stable daughter isotope. As applied to lunar evolution, such events can include small-scale processes, such as the crystallization of an igneous rock, to global scale processes such as the formation of the mantle reservoirs that served as the sources of mare basalts.

The requirements for a radiometric approach to provide an accurate and chronologically significant age are easily stated but often not easily verified in real samples. The primary requirements are that the:

- decay of a radioactive parent isotope creates a sufficient change in the isotopic composition of the daughter element to be precisely determined
- parent/daughter element ratio of the sample being dated does not change after the time of sample formation
- isotopic composition of the daughter element is affected only by decay of the parent isotope

The last point involves the concept of "closure temperature" that reflects the fact that at high temperatures, diffusion of an element within a crystal lattice can cause either loss of the radiogenic component from the crystal or its dilution by isotopically distinct daughter element diffusing into the mineral from its surroundings. The closure temperature is highly variable between various isotopic systems and in different minerals because it is function of a variety of parameters including the distinct diffusional properties of the parent and daughter elements, the duration of heating the rock experienced, and the size of mineral grains that comprise the rock (e.g., Dodson 1973). Age spectra produced by the Ar-Ar dating method are a direct measure of the diffusive loss of radiogenic ^{40}Ar as the different temperature steps involved in the measurements are, in essence, extracting ^{40}Ar from crystallographic sites in the sample that have different closure temperatures (e.g., McDougall & Harrison 1999). Constant Ar-Ar ages over a wide range of extraction temperatures give confidence that the age obtained is accurate but does not unambiguously distinguish whether the event being dated is the original crystallization age of the sample or the time of a later metamorphic event that caused extensive outgassing of radiogenic ^{40}Ar from the sample. Argon is a noble gas and is easily mobilized during heating at relatively low temperatures in response to metamorphism occurring on the lunar surface and thus is commonly used to date impact metamorphism (e.g., Stoffler et al. 2006). While Ar-Ar can give accurate crystallization ages for rocks that have not experienced heating events after formation, few ancient rocks from the lunar highlands meet this criterion. Argon-argon dates for lunar highlands samples thus tend towards younger ages than those determined by systems with higher closure

temperatures. Consequently, this discussion is focused on chronometric systems such as Rb-Sr, Sm-Nd, Lu-Hf, and U-Pb that are less easily reset by impact heating events. Short duration thermal events associated with impacts tend to either not mobilize or only partially mobilize these elements, at worst disturbing, but not resetting, the isochrons that define the crystallization ages of the rocks (Gaffney et al. 2011). Prolonged residence of a sample at high temperatures, however, causes these chronometers to provide "cooling ages". Such ages reflect not the time of sample crystallization, but instead the time when the sample cooled below the temperature where diffusion of the daughter isotope between minerals can occur. If the sample is quickly brought to the surface by a large impact from an elevated temperature where diffusion was occurring, the age provided by the chronometer may indicate when it was excavated from the deep lunar crust and not the original igneous crystallization age (e.g., McCallum et al. 2006, Marks et al. 2019).

3. FACTORS AFFECTING Rb-Sr, Sm-Nd, AND Lu-Hf ISOCHRON AGES

An isochron requires a minimum of two subsamples that have different parent/daughter element ratios to form a line on a plot of daughter isotopic composition versus parent/daughter ratio. As two points always define a line, adding additional points to the isochron and showing that all measurements lie within analytical uncertainty of a single line helps make the case that the line indeed is an isochron with chronological significance. Obtaining multi-point isochrons is often possible for mare basalts that have many mineral phases present. Obtaining multi-point isochrons, however, is not always possible for ancient lunar crustal rocks because many are so strongly dominated by a single mineral, plagioclase, that finding even a second mineral that can be used to define the isochron is a challenge.

There are several ways to evaluate whether a given age represents a crystallization event (see review in Borg et al. 2015). For example, the characteristics of an individual isochron regression provide insights into the reliability of the ages that they define. Large uncertainties in the calculated ages reflect poorly defined isochron slopes reflective of either limited differences in parent/daughter ratios in the fractions used to construct the isochron or significant scatter in the data, potentially indicative of disturbance of the chronometer. Scatter of the data about a best fit line is most often quantified using the mean squared weighted deviation (MSWD). This statistical parameter reflects the degree to which individual data points fit the calculated regression of the data, taking into account the analytical uncertainties associated with the data. A good fit of Sm-Nd isotopic data to a regression is reflected by MSWDs of approximately 1, whereas values higher than approximately 5 are usually deemed to indicate a poor fit (Wendt & Carl 1991). The initial Nd isotopic composition provided by the isochron also allows the reliability of the isochron age to be estimated by quantifying the REE systematics of the source from which the dated rock is derived. In some cases, the initial Nd isotopic compositions determined for FAS samples are very high, suggesting derivation from sources that were strongly depleted in LREE relative to HREE

for tens to hundreds of millions of years prior to crystallization of the FAS sample. Derivation of FAS from such a reservoir, however, is inconsistent with petrologic models of LMO differentiation that predict crystallization of plagioclase-rich rocks relatively early in the LMO crystallization sequence from magmas that experienced minimal REE elemental fractionation and therefore have chondritic to slightly LREE-enriched REE abundances. Finally, the most reliable indicator that an age determination is correct is to obtain the same age on the same mineral and whole rock fractions using a different isotopic system. The premise is that open system processes that contaminate the sample or mobilize parent and daughter isotopes are unlikely to do so in such a way as to yield concordant ages from two chronometers based on geochemically dissimilar elements. Unfortunately, only a handful of chronologic investigations completed on highlands samples have been successful in obtaining concordant ages from multiple isotopic systems.

3.1. Impact metamorphism

Given the large range of reported ages of FAS and Mg-suite samples, the key question is whether this age range accurately reflects the duration of lunar crust formation or instead disturbance of isochron systematics by one of several factors that commonly affect ancient lunar crustal rocks. The most obvious cause of disturbance is the shock metamorphism experienced to at least some degree by essentially all ancient rocks from the lunar highlands. Experimental investigations documenting the response of the Rb-Sr, U-Pb, and Sm-Nd isotopic systems to both high shock pressure (55 GPa) and high temperature (1000 °C) demonstrate that conditions associated with impact metamorphism do not yield linear isochron plots with erroneous ages (Gaffney et al. 2011). Furthermore, diffusion coefficients for some elements (e.g., REE) are very low, requiring long duration high temperature events in excess of ~850 °C to re-equilibrate daughter isotopes (e.g., ^{142}Nd and ^{143}Nd) between plagioclase and pyroxenes (Cherniak 2003, McCallum et al. 2006, Cherniak & Liang 2007). In other words, impact metamorphism does not appear to reset ages by "rotating" isochrons. Instead, thermal metamorphism produces scatter on isochron diagrams by affecting the minerals with low-closure temperatures more than those with high-closure temperatures. A likely culprit in this process is the maskelynitization of plagioclase observed in many highland samples that reflects the conversion of plagioclase to an amorphous form, likely drastically increasing the diffusion coefficients of its constituent elements thereby effectively lowering its closure temperature.

The Rb-Sr chronometer provides a clear demonstration of how most (all but Ar-Ar) isotope systems respond to impact metamorphism. Rubidium-strontium isotope measurements have been completed in conjunction with Sm-Nd isotopic measurements on FAS samples 60016, 60025, 62236, 62237, 67016, and 67215 (Carlson & Lugmair 1988, Alibert et al. 1994, Snyder et al. 1994, Borg et al. 1999, Norman et al. 2003, Nyquist et al 2006, Sio et al 2020, Marks et al. 2019) and are plotted in Supplemental Figure 1. From Supplemental Figure 1 it is obvious that mobilization of Rb from the minerals as a result of impact metamorphism is why this chronometer has met with

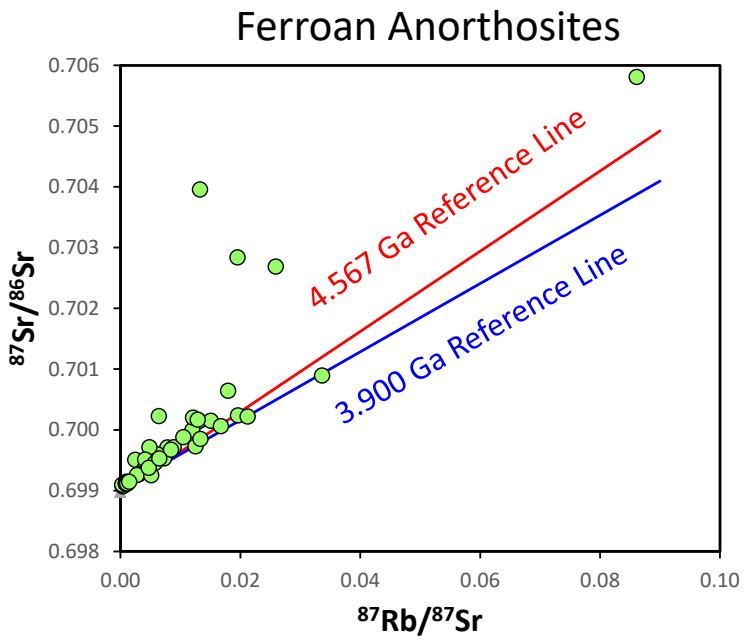

Supplemental Figure 1. *Compilation of Rb-Sr isotopic data measured on FAS samples and mineral fractions. Red line is 4.567 Ga reference line passing through the Solar System initial Sr isotopic value. Blue line is 3.90 Ga reference line passing though bulk Moon $^{87}Sr/^{86}Sr$ value calculated from the Solar System initial $^{87}Sr/^{86}Sr$ value assuming $^{87}Rb/^{86}Sr = 0.019$. Data from (Carlson & Lugmair 1988, Alibert et al. 1994, Snyder et al. 1994, Borg et al. 1999, Norman et al. 2003, Nyquist et al. 2006, Sio et al. 2020, Marks et*

limited success in dating FAS samples. Many mafic mineral fractions (those with elevated $^{87}Rb/^{86}Sr$ ratios) lie to the left of the 4.567 Ga reference isochron indicating that they have lost Rb. A temporal constraint for the timing of this disturbance is probably recorded in the Rb-Sr data because much of the data fall along a line with a slope corresponding to an age of ~3.9 Gyr. This implies that redistribution of Rb-Sr in many of these samples occurred at the time of the Imbrium impact (Borg et al. 1999, Norman et al. 2003, Nyquist et al. 2006). However, this age is not manifested by an isochron in any single set of Rb-Sr data and would probably not be identified from the data without prior knowledge of the Imbrium impact age.

3.2. Combining data for unrelated lithologies

Although heating and shock associated with impacts are unlikely to result in erroneous age determinations, there are other processes associated with impacts that could. For example, analysis of a lithic breccia composed of two distinct lithologies and petrographically misinterpreted as a monomict brecciated rock could yield linear arrays on isochron diagrams that have no age significance. Petrographic evidence for such mixed lithologies is subtle because elemental disequilibrium is not a clear indicator of isotopic disequilibrium. For example, minerals derived from the same parental magma at different stages of crystallization will have elemental compositions that are not in chemical equilibrium, and yet will lie on the same isochron defining the age of the sample. Thus, chemical disequilibria between minerals defining an isochron does not necessarily preclude the isochron from recording the age of the sample.

The presence of impact melt is almost ubiquitous in FAS samples. The impact melt is often splashed onto the surface of the samples and injected as veins into the interior. The impact melt is typically depleted in volatile elements such as Rb and Pb, and can be, although not always, derived from materials that were foreign to the sample. In FAS samples, the impact melt is dark in color and is found along pyroxene/olivine-plagioclase grain boundaries and is therefore very difficult to separate from dark mafic minerals by hand-picking. Furthermore, pyroxene and olivine have very low modes in FAS samples so that in order to obtain enough mafic minerals for an analysis, less pure mafic mineral separates must often be accepted. As a result, some isochrons for highlands samples may include data that are a mixture of the original igneous minerals in the rock with extraneous impact melt that would cause the data to fall off the true isochron resulting in scatter and best fit lines that correspond to inaccurate ages.

3.3. Slow cooling

Understanding the thermal history of each sample being dated is important because slowly cooled plutonic rocks on the Moon cool at rates of only a few °C/Myr. Therefore, a rock intruded into the crust near or above its solidus temperature can stay above the closure temperature of Sm-Nd diffusion in plagioclase and pyroxene for tens of millions of years (McCallum et al 2006). For example, the emplacement age of 60025 has been estimated to be ~16 Myr older than the measured crystallization age because this rock is thought to have cooled at ~18 °C/Myr (McCallum & O'Brien 1996) from its solidus temperature of ~1150°C to the temperature at which diffusion ceased around 825 °C (Borg et al 2017). In the case of very slowly cooled samples the difference between measured age and emplacement age can be even larger. For a sample like Mg-suite troctolite 76535, that cooled around 5 °C/Myr, the age recorded by Sm-Nd might post-date emplacement of the magma in the crust by 80 Myr.

3.4. Cosmic ray exposure

Many rocks from the lunar highlands have resided close enough to the lunar surface for long enough to have experienced significant interaction with energetic cosmic rays and the thermal neutrons that they generate within the lunar regolith. The consequence is isotopic modification of the elements used in chronometric systems by a combination of spallation and capture of thermal and epithermal neutrons by the element and those close to it in mass.

Neutron capture affects the Sm-Nd isotopic system by modifying the isotopic composition of ^{142}Nd, ^{149}Sm, and ^{152}Sm with only limited direct impact on ^{143}Nd. The largest neutron capture effect is on ^{149}Sm because it has a very large neutron capture cross section. Most Sm-Nd measurement techniques use isotopically enriched ^{149}Sm to calculate the amount of ^{147}Sm in the sample using the isotope dilution method. By modifying the ^{149}Sm isotopic composition of the sample, neutron capture can result in erroneous ^{147}Sm/^{144}Nd ratios unless a separate measurement

is made of the unspiked Sm isotopic composition so that the correct abundance of ^{149}Sm can be used to calculate the correct Sm concentration in the sample. The problem is further compounded for FAS in that the proportion of ^{152}Sm in samples characterized by high abundances of plagioclase is also strongly affected by neutron capture because this isotope is produced by capture on ^{151}Eu which is highly abundant in plagioclase-rich samples. Production of ^{152}Sm in FAS samples is important because Sm isotopes are commonly measured relative to ^{152}Sm (e.g., ^{149}Sm/^{152}Sm), and this effect is easily overlooked. An issue introduced by having to run spiked and unspiked splits of the sample is the requirement that the two sample splits are compositionally identical so that the parent/daughter ratios measured in the spiked split corresponds precisely to the daughter isotopic composition measured in the unspiked split. This is a particular problem for aluminum-rich FAS samples because after dissolution they often contain small amounts of nearly invisible precipitates that, under examination using a secondary electron microscope, contain variable proportions of Sm and Nd. A final consequence of cosmic ray exposure is direct modification of Nd isotopic composition. Both ^{145}Nd and ^{142}Nd can experience significant modification at high cosmic ray exposure. For example, the ^{142}Nd/^{144}Nd ratio of FAN 62236 had to be corrected by 16 ppm (Boyet et al. 2015) while some mare basalts need correction of up to 35 ppm (Brandon et al. 2009; Borg et al., 2019). For reference, the total variation in ^{142}Nd/^{144}Nd seen in all lunar samples is roughly 60 ppm, so the cosmic ray corrections for samples with long exposure histories can be very significant and likely explain much of the scatter seen in Figure 7 of the main text. Detailed mathematical treatments for correction of neutron capture can be found in (Nyquist et al. 1995, Borg et al. 1999, 2019, Brandon et al. 2009, Gaffney & Borg 2014), but these corrections depend on the cumulative energy spectrum of the neutrons which interacted with the sample, which cannot be determined precisely.

Cosmic ray exposure has equally, if not more severe, consequences for the Lu-Hf system (Sprung et al 2010, Sprung et al 2013). For Hf in lunar samples, the primary consequence of cosmic ray exposure is a decrease in ^{177}Hf by neutron capture to ^{178}Hf that results in higher measured ^{176}Hf/^{177}Hf. Correcting for this effect can be done by estimating the exposure age from offsets in ^{180}Hf and ^{149}Sm abundances that respectively provide measures of the

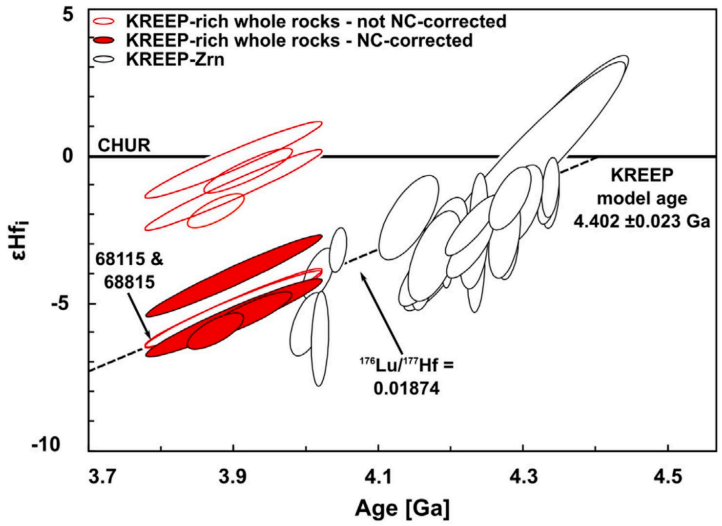

Supplemental Figure 2: Initial Hf isotope data for KREEP rich samples before (open ellipses) and after (filled ellipses) correction for cosmic ray effects (Sprung et al. 2013). Also included in this figure are data for the initial Hf isotopic composition, uncorrected for cosmic ray exposure, of lunar zircons (Taylor et al. 2009).

epithermal and thermal neutron flux experienced by the sample. The effect can be as large as 5 parts in 10,000 on the $^{176}Hf/^{177}Hf$ ratio, which is enough to cause model ages for some KREEP samples with long cosmic ray exposures to change from 3.9 Gyr to 4.4 Gyr (Supplemental Figure 2).

Given all these potential complications of radiometric age determinations for lunar samples, the best way to demonstrate that an isochron represents the crystallization age of a sample is to confirm the age using a second isotopic system because diffusion of isotopes in the mineral phases, mixing of extraneous minerals into the rock, and cosmic ray effects are highly unlikely to result in concordant but inaccurate ages in two or more independent systems.

4. APPLICATION OF THE U-Pb SYSTEM TO LUNAR CHRONOLOGY

The U-Pb system is a very powerful dating tool, but in lunar applications is often complicated because of the very low Pb contents of most lunar rocks as a result of the general depletion of the Moon in volatile elements. In contrast, U is a highly refractory element, so the Moon has a bulk U/Pb ratio some 250 to 1300 times higher than chondritic (Tatsumoto 1970, Snape et al. 2016). This is most obviously seen in the estimates of the initial Pb isotopic composition of ancient lunar highland rocks, such as for the Apollo 15 anorthosite 15415 (Tera et al. 1974) as shown in Supplemental Figure 3. On this plot, the intercept of the line defined by the variety of highlands samples extrapolates to $^{207}Pb/^{206}Pb = 1.45$ at a $^{238}U/^{206}Pb = 0$, a value that is significantly higher than the initial $^{207}Pb/^{206}Pb$ of the Solar System of 1.1076 (Blichert-Toft et al. 2010). Starting at the initial Solar System value, $^{207}Pb/^{206}Pb$ ratios of 1.45 can only be obtained in reservoirs with $^{238}U/^{204}Pb$ ratios above 90, which is very high compared to the CI-chondrite value of 0.19. Furthermore, to preserve the high $^{207}Pb/^{206}Pb$ ratio of this component it must be isolated from further contributions from U decay occurring after about 3.9 Gyr. The line defined by the highland samples in Supplemental Figure 3 reflects the widespread presence of this very high initial $^{207}Pb/^{206}Pb$ component in lunar highland samples. Samples with high enough U/Pb to sufficiently overprint this initial Pb plot closer to the concordia curve as shown in the inset to Supplemental Figure 3. The origin of this unsupported high $^{207}Pb/^{206}Pb$ is not clear. It appears in soils and as a leachable surface component on some lunar samples which suggests it could be Pb that was vaporized by a particularly energetic event, such as a basin-forming impact, and redeposited on the lunar surface. That the line in Supplemental Figure 3 extrapolates to a lower intercept age of 3.9 Gyr led to the suggestion that this intercept reflects a time of extensive bombardment of the lunar surface, the so-called terminal cataclysm (Tera et al. 1974), although a single large impact, such as the one that formed the Imbrium Basin, could create the same U-Pb systematics. The correlation line shown in Supplemental Figure 3 also crosses concordia at 4.42 Gyr that was interpreted by (Tera et al. 1974) either as the formation age of the Moon or the crust of the Moon, or alternatively a chronologically meaningless number caused by mixing between the fugitive Pb

end member characterized by a $^{207}Pb/^{206}Pb$ of 1.45 with Pb generated by U decay after the 3.9 Gyr event.

The high U/Pb of the Moon should allow this system to provide precise chronological results for lunar samples, and in many cases, it has, but the low Pb concentration of many lunar crustal rocks makes the samples susceptible to Pb contamination both from lunar Pb that was volatilized by impacts and redeposited on samples exposed at the surface, and from terrestrial Pb. Given the care with which the Apollo samples were collected and preserved prior to analysis, how modern terrestrial Pb got into the samples is a good question, but the fact that weak acid leaches of lunar samples often provide Pb with isotopic compositions indistinguishable from terrestrial Pb was a problem recognized very early in lunar sample analysis (Tera et al. 1974, Unruh et al. 1977) and has not gone away even as laboratory blanks improved (Borg et al. 2011).

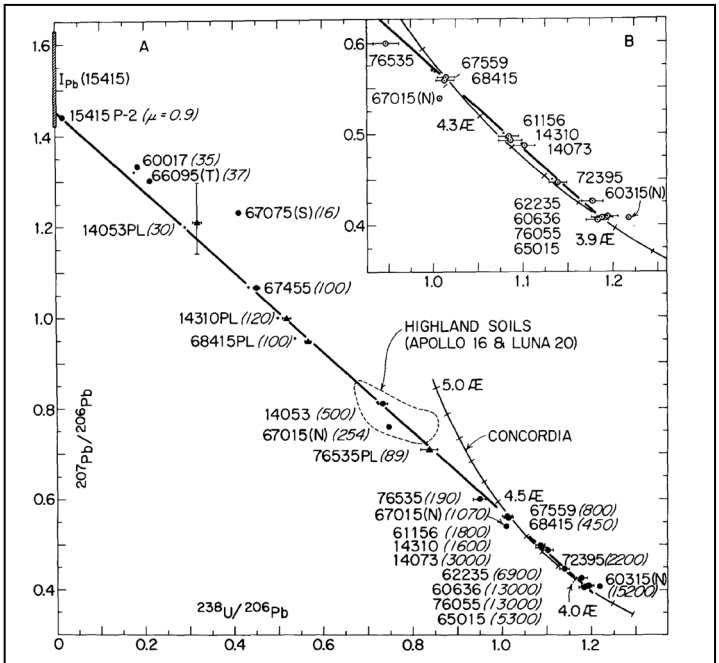

Supplemental Figure 3: Inverse concordia diagram plotting the U-Pb data for a number of highland rocks and soils. Figure from (Tera et al. 1974)

The high bulk U/Pb ratio of the Moon and the impact of fugitive Pb components in the analysis of lunar samples impacts the chronological results obtained from lunar samples in two ways. First, since the single-stage Pb isotope model age of modern terrestrial Pb is near 4.4 Gyr (Patterson 1956, Stacey & Kramers 1975), mixtures of terrestrial Pb contamination with the indigenous Pb in the lunar sample can form mixing lines on $^{207}Pb/^{206}Pb$ versus $^{204}Pb/^{206}Pb$ plots that can be mistaken for isochrons, often with ages near 4.4 Gyr, that in reality have no age significance. Second, the presence of the high $^{207}Pb/^{206}Pb$ component in many lunar highlands samples can draw sample analyses off of the Pb-Pb isochron causing scatter in the data and leading to artificially young ages if those data are included in the isochron line fitting. The Pb data for Apollo 16 anorthosite 60025 (Tera & Wasserburg 1972, Hanan & Tilton 1987, Borg et al. 2011) provide a good example of both problems as discussed in the main text and shown in Figure 8. Both problems can be overcome in minerals with good Pb retention (high closure temperature) and high U/Pb ratios, i.e., zircon. Lunar zircons have provided precise U-Pb ages (Meyer et al. 1996, Nemchin et al. 2006, 2008, 2009, Pidgeon et al. 2007, Taylor et al. 2009, Grange et al. 2009, 2011, Barboni et al. 2017), but

as the majority of lunar zircons are essentially detrital grains, connecting these ages directly with the major rock forming units of the ancient lunar crust is not possible.

5. MODEL AGE SYSTEMATICS

The isotopic composition of the daughter element in a radioactive decay system integrates the cumulative result of all the changes to the parent/daughter ratio that have occurred not only in the sample, but potentially also in the materials from which the sample formed. When the daughter element is completely lost from the system, for example when Ar outgasses from an erupting magma or a zircon strongly excludes Pb during crystallization, the prior history of the materials that gave rise to the magma is completely lost. For systems where the degree of parent/daughter element fractionation is not so extreme, the isotopic composition of the daughter element at the time of formation of the rock retains information about the history of the material from which the rock formed. Comparing the initial isotopic characteristics of a rock with a model for the isotopic evolution of its source can produce a "model age" that can reveal the timing of events that predate the formation of individual rocks. A model age, however, is only as accurate as the model it is based on. As model ages play a large role in estimating the timing of major lunar differentiation events, particularly LMO crystallization, understanding the dependency of these ages on model assumptions is critical to their correct interpretation.

5.1. Comparing lunar and terrestrial ^{182}W

High precision W isotope data show the Moon to have a $^{182}W/^{184}W$ ratio some 20 to 27 ppm higher than that estimated for the present day bulk silicate Earth (Supplemental Figure 4): Kruijer et al. 2015, Touboul et al. 2015, Kruijer & Kleine 2017), which in turn is about 200 ppm higher than the W isotopic composition of average chondrites (Kleine et al. 2009). As core formation causes an increase in the Hf/W ratio of the silicate portion of the planet because core Hf/W ratios are essentially 0, the superchondritic $^{182}W/^{184}W$ of Earth, Moon, and Mars potentially reflect core formation on these planetary objects while ^{182}Hf was still extant (Kleine et al. 2002, Yin et al. 2002). Turning these data into the age of core formation is complicated by the likelihood that core formation is not a single event, but instead occurred as a result of the melting associated with every large impact during planet growth (Nimmo & Agnor 2006). For Earth, a simple single stage Hf-W model age for core formation is of the order 30 Myr after Solar System formation, but this age can extend to 100+ Myr depending on the details of the core formation process (Kleine et al. 2009). Given the similar, but not identical, W isotopic composition of Earth and Moon, a similar timescale might be applied to core-mantle separation during Moon formation. However, the Hf-W data do not clearly discriminate whether this metal-silicate separation occurred on the Moon after its formation or instead in the materials from which the Moon formed, for example, the proto-Earth and Theia.

On the basis of new analyses of the trace element composition of lunar samples, Thiemens et al. (2019) argue that the bulk Hf/W ratio of the Moon (30-48) is higher than that of the silicate Earth (26). On the assumption that the difference in W isotopic composition between Earth and Moon reflects ingrowth of additional ^{182}W due to the higher Hf/W ratio of the Moon, these authors suggest that the Moon must have formed within 50 Myr of Solar System formation, or prior to 4518 Myr. This interpretation is controversial. Kruijer et al. (2021) note that in a giant impact model, the W isotopic composition of the Moon would be a mixture of the W from the proto-Earth and Theia which would imply that Earth and Moon need not have started with the same $^{182}W/^{184}W$, and even if they did, late additions of chondritic material to Earth after Moon formation could have lowered Earth's $^{182}W/^{184}W$ to the modern value (Bottke et al. 2010, Kruijer et al. 2021) independent of any contribution from ^{182}Hf decay. Adding to the uncertainty in this approach is that the $^{182}W/^{184}W$ of rocks from Earth increase with age so that values for Archean rocks approach those of the lunar samples. One explanation for the cause of the W isotope variability in terrestrial rocks is the continuing addition of late accreting chondritic materials to Earth's mantle (Willbold et al. 2011, Touboul et al. 2014). However, this explanation is hard pressed to explain the variability in W isotopic composition in modern ocean island basalts (Supplemental Figure 4: Mundl et al. 2017), particularly in light of the evidence for efficient mantle mixing provided by the decline in $^{142}Nd/^{144}Nd$ variability in terrestrial rocks by ~2.7 Gyr (Carlson et al. 2019). An alternative is that the terrestrial variability in W isotopic composition reflects exchange between Earth's core and mantle through time (Rizo et al. 2019) as the core also is expected to have a very low $^{182}W/^{184}W$. Whatever the explanation for the terrestrial variability, examination of the range in W isotope data shown in Supplemental Figure 4 illustrates the care that should be exercised in interpreting the cause of the difference between terrestrial and

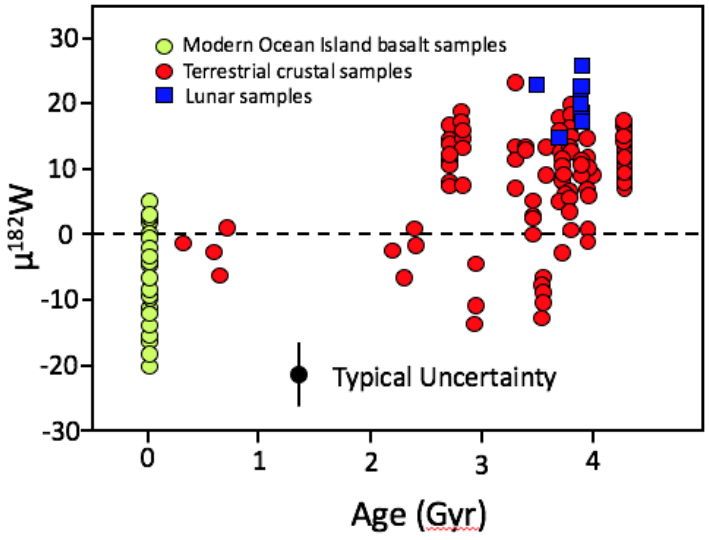

Supplemental Figure 4. *Variation in $^{182}W/^{184}W$ through time for lunar and terrestrial rocks including modern ocean island basalts (OIB). The W isotopic composition is expressed in μ units that indicate the difference in $^{182}W/^{184}W$ from the terrestrial standard in parts per million. Lunar data from Touboul et al. (2015), Kruijer et al. (2015), Kruijer & Kleine (2017) and for terrestrial rocks from Willbold et al. (2011, 2015), Touboul et al. (2012, 2014), Rizo et al. (2016, 2019), Liu et al. (2016), Puchtel et al. (2016, 2018), Mundl et al. (2017,*

lunar W isotopic composition, and particularly in turning that difference into an age estimate for Moon formation.

5.2. Sm-Nd evolution of the lunar interior

Supplemental Figure 5 illustrates how the model age approach can provide useful information about the Moon's early differentiation as well as how that information can be misleading. If the lunar interior had not experienced differentiation, it would have a chondritic Sm/Nd ratio because both elements are refractory lithophile elements, meaning that they would not be fractionated by condensation or evaporation or by partitioning between core and mantle. A chondritic starting point for the Moon thus is the first assumption in this model. While likely to be true, this assumption may be incorrect if, for example, the Moon formed preferentially from already differentiated crustal materials on Earth and Theia. Some have suggested that the LMO may have been characterized by a subchondritic Sm/Nd ratio (Nyquist et al 1979), thus introducing uncertainty on the basic assumption of this model age approach. If the lunar interior did start with a chondritic Sm/Nd ratio, then a magma derived by melting of the lunar interior, no matter when that melting took place, would

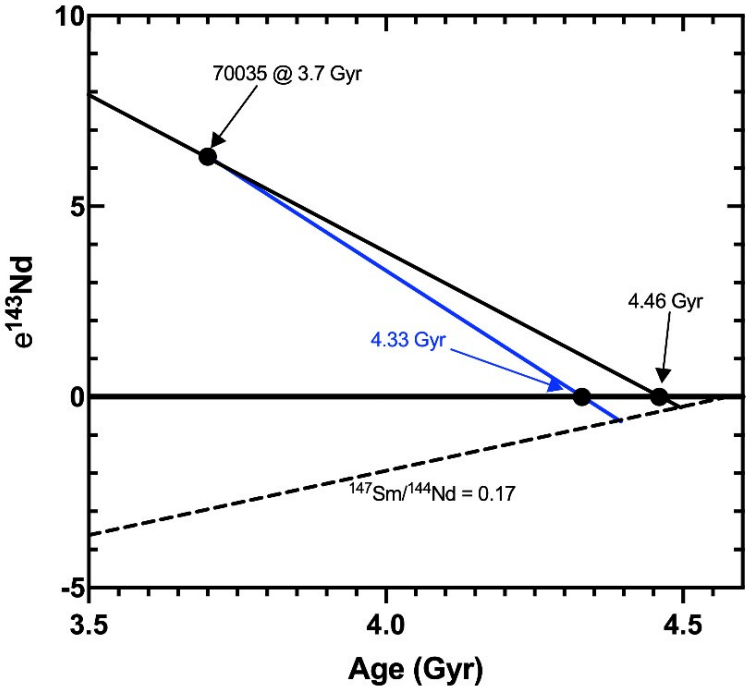

Supplemental Figure 5. *Model evolution of Nd isotopic composition using the data for 70035* (Borg et al 2019) *as an example. From the starting point of the measured whole rock Sm/Nd, extrapolating the measured $^{143}Nd/^{144}Nd$ backwards leads to the thin black line that passes through the initial $\varepsilon^{143}Nd$ of +6.3 for this sample at 3.7 Gyr. That line continues to intersection with chondritic evolution ($\varepsilon^{143}Nd = 0$) at 4.46 Gyr. If the melting event that produced the 70035 parental magma caused a 5% decrease in Sm/Nd in the magma compared to the source, the higher source Sm/Nd would lead to the evolution shown by the thin blue line, providing a chondritic model age of 4.33 Gyr. If the bulk Moon has a subchondritic $^{147}Sm/^{144}Nd = 0.17$ (Nyquist et al. 1979), these model ages would increase to 4.49 and 4.36 Gyr, respectively.*

have the same $^{143}Nd/^{144}Nd$ as a chondrite at the time of magma genesis. This is clearly not the case for some types of mare basalts. High-Ti mare basalts from both Apollo 12 and 17 had strongly superchondritic $^{143}Nd/^{144}Nd$ at the time of their eruption. In contrast, aluminous mare basalts had initial $^{143}Nd/^{144}Nd$ close to or just slightly above chondritic, and the incompatible element rich lunar rock type called KREEP-basalts had sub-chondritic $^{143}Nd/^{144}Nd$ at the time of eruption. The compositional differences between different groups of mare basalts testify to their genesis from compositionally distinct sources in the lunar interior.

Following one of the first applications of the Sm-Nd system (Lugmair et al. 1975) as an example of how a model age can be calculated, the high-Ti mare basalt 70035 has a measured $^{147}Sm/^{144}Nd = 0.25898$ and $^{143}Nd/^{144}Nd = 0.514494$ (Borg et al. 2019) compared to average chondritic $^{147}Sm/^{144}Nd = 0.1960$ and $^{143}Nd/^{144}Nd = 0.512630$ (Bouvier et al. 2008). Given the superchondritic Sm/Nd and $^{143}Nd/^{144}Nd$ of 70035, its Nd isotopic composition will converge with chondritic Nd isotopic composition at some time in the past (Supplemental Figure 5). Using its measured Sm/Nd to extrapolate its Nd isotopic composition back in time, at the 3.7 Gyr age of eruption age of 70035, its $^{143}Nd/^{144}Nd$ was still well above chondritic. This is indicated by a positive initial $\varepsilon^{143}Nd$ of +6.3 where $\varepsilon^{143}Nd$ is defined as:

$$\varepsilon 143Nd(t) = \left[\frac{\frac{^{143}Nd}{^{144}Nd}_{Sample}}{\frac{^{143}Nd}{^{144}Nd}_{Chondrite}} - 1 \right] \times 10{,}000$$

The positive initial $\varepsilon^{143}Nd$ determined for 70035 is evidence of its derivation by melting of a source rock that had superchondritic Sm/Nd for a long time prior to the melting event. This is not a startling conclusion given the substantially superchondritic measured Sm/Nd of 70035. When the source of 70035 developed its superchondritic Sm/Nd ratio can be estimated using the model age approach. The simplest model uses the measured whole rock Sm/Nd of 70035 to calculate the measured $^{143}Nd/^{144}Nd$ back to a time when it intersects the evolution of a material with chondritic Sm/Nd. The equation to calculate this type of Sm-Nd model age is:

$$T_{Model} = \frac{1}{\lambda_{Sm}} \times ln \left[\left[\frac{\left(\frac{^{143}Nd}{^{144}Nd}\right)_{Model} - \left(\frac{^{143}Nd}{^{144}Nd}\right)_{Sample}}{\left(\frac{^{147}Sm}{^{144}Nd}\right)_{Model} - \left(\frac{^{147}Sm}{^{144}Nd}\right)_{Sample}} \right] + 1 \right]$$

where λ_{Sm} is the decay constant of ^{147}Sm (6.54×10^{-12} yr^{-1}). Using the chondritic parameters for "model" and the whole rock data for 70035 for "sample" in the equation above, the model age is 4.46 Gyr (Supplemental Figure 5). This result implies that the source of 70035 had its composition established some 640 Myr prior to the melting event that produced the basalt or just 100 Myr after Solar System formation.

The model age calculated above involves only two stages in the evolution of Nd in 70035. The first stage is evolution with chondritic Sm/Nd from 4.567 Gyr to 4.46 Gyr, the second involves evolution with superchondritic Sm/Nd from 4.46 Gyr to the present day. The two-stage model neglects the third-stage that occurred when partial melting that produced the parental magma of 70035 changed the Sm/Nd of the melt compared to its source. Given that Nd generally is more incompatible than Sm during partial melting, the Sm/Nd measured in 70035 likely is lower than it was in the source of the magma. If the Sm/Nd of 70035 is, for example, 5% lower than the Sm/Nd of its source, the true $\varepsilon^{143}Nd$ isotope evolution path prior to 3.7 Gyr would be steeper than if calculated using the measured Sm/Nd of 70035 (Supplemental Figure 5). As a result, the 4.46 Gyr model age for the source would decrease to 4.33 Gyr (Supplemental Figure 5). This 160 Myr change in the calculated model age provides an illustration of the sensitivity of model ages to the parameters used to model the evolution of the source of the sample. With each addition of another evolutionary stage, more parameters are introduced whose exact values cannot be determined. While these more complicated evolutionary models likely do a better job of approximating reality, the uncertainties in composition within each evolutionary stage contribute to increase the uncertainty of any model age obtained.

The example above used only the ^{147}Sm-^{143}Nd system, but source evolution models will also affect other radiometric systems such as Lu-Hf and Rb-Sr. Inaccuracies in model assumptions are likely to affect the different systems in different ways, so consistency in the model ages from the different systems lends support to the answer provided. This comparison between different systems has been most effectively used by combining the ^{147}Sm-^{143}Nd and ^{146}Sm-^{142}Nd systems in order to refine the accuracy of Sm-Nd model ages for the timing of LMO crystallization (Nyquist et al. 1995, Boyet & Carlson 2007, McLeod et al. 2014, Borg et al. 2019). Given the 103 Myr half-life of ^{146}Sm, this system effectively goes extinct by ~4 Gyr so that the $^{142}Nd/^{144}Nd$ measured today in a 3.7 Gyr basalt is essentially the same as it was when the rock formed. With combined $^{146,147}Sm$ – $^{142,143}Nd$ measurements, two estimates of a sample's Sm/Nd history can be inferred; one (^{146}Sm-^{142}Nd) of which is insensitive to any change to the source's Sm/Nd that occurs after ~4 Gyr, while the other (^{147}Sm-^{143}Nd) integrates the consequences of every change in Sm/Nd experienced by the sample up to the present day.

In the example for 70035 given above, a source for the 70035 magma that evolved from 4.567 Gyr to 4.46 Gyr with chondritic Sm/Nd and bulk-Earth $^{142}Nd/^{144}Nd$ and then with the same Sm/Nd as the 70035 whole rock from that point until today would have a $\mu^{142}Nd = +46$ where $\mu^{142}Nd$ is defined as:

$$\mu 142Nd(t) = \left[\frac{\frac{^{142}Nd}{^{144}Nd}_{Sample}}{\frac{^{142}Nd}{^{144}Nd}_{Model}} - 1 \right] \times 10^6$$

The measured μ^{142}Nd of 70035 is +8, which implies either that the source model age is too old, the Sm/Nd measured for 70035 is higher than it was in its source rock, or both. Partial melting generally results in a lower Sm/Nd in the melt than the source, so looking to a younger age for source formation is the more likely option in this case. For example, using the measured Sm/Nd for 70035, a source model age of 4.2 Ga would lead to a μ^{142}Nd = +8 and an initial ε^{143}Nd = +4.2 at 3.7 Ga, with the latter value being slightly lower than the +6.3 determined for 70035. In this case, there is no combination of source Sm/Nd and age of source formation that can simultaneously satisfy both the ε^{143}Nd and μ^{142}Nd data for 70035, indicating that this simple model for source formation, or one or more of the parameters in the model, is incorrect.

A third variable that is important in these calculations is the value of ^{142}Nd/^{144}Nd assumed for the bulk-Moon. Although originally assumed to be constant in the Solar System, the ^{142}Nd/^{144}Nd ratio is now known to display significant – tens of ppm – variation due to imperfect mixing of nucleosynthetically distinct elemental contributions to the Solar System (Carlson et al. 2007, Gannoun et al. 2011, Burkhardt et al. 2016, Fukai & Yokoyama 2017, Saji et al. 2020). For example, ^{142}Nd/^{144}Nd in modern terrestrial rocks is some 20 ppm higher than in average ordinary chondrites and up to 45 ppm higher than some carbonaceous chondrites. The only meteorite group with ^{142}Nd/^{144}Nd close to overlapping modern terrestrial values is enstatite chondrites (Gannoun et al 2011), but only a subset of that group has ^{142}Nd/^{144}Nd as high as the present Earth (Boyet & Gannoun 2013). Given the very small contribution of ^{146}Sm decay to ^{142}Nd, if the bulk-Moon ^{142}Nd/^{144}Nd is ~10 ppm lower than the current bulk-Earth value (Sprung et al 2013, Carlson et al 2014, Borg et al 2019), then a source formation age of 4.32 Ga would result in the source of 70035 having a μ^{142}Nd = +8 (+18 relative to a bulk-Moon μ^{142}Nd of -10) and initial ε^{143}Nd = +5.2 and thereby provide a better match to the measured data.

5.3. Whole rock isochrons for mare basalts

Where the combination of the two Sm-Nd systems (^{146}Sm-^{142}Nd and ^{147}Sm-^{143}Nd) has been particularly useful for lunar chronology is in refining the Sm/Nd ratios used to model the production of the mare basalt sources during LMO crystallization and plotting this value against the measured ^{142}Nd/^{144}Nd ratios to obtain model ages for the formation age of the mare basalt sources (Figure 7 in main text). If these chemically distinct sources formed in a single event long before the eruption age of the basalts themselves, and parent/daughter elemental fractionation did not occur during the melting event that produced the basaltic magmas, then a ^{147}Sm-^{143}Nd isochron

(plotted as $^{147}Sm/^{144}Nd$ versus $^{143}Nd/^{144}Nd$) or a ^{146}Sm-^{142}Nd isochron (usually plotted as $^{147}Sm/^{144}Nd$ versus $^{142}Nd/^{144}Nd$) constructed from the whole rock data for the compositionally distinct mare basalts would provide the age of this initial source formation event (Supplemental Figure 5). However, although mare basalt whole rock radiogenic isotope data do, for the most part, define linear relationships on Sm-Nd isochron diagrams, some parent/daughter fractionation most likely occurs during melting. As a result, plotting whole rock data generally does not accurately constrain the formation age of the mare basalt sources. In fact, such ages can be inaccurate by hundreds of millions of years for the ^{147}Sm-^{143}Nd system (Supplemental Figure 6). Because of the shorter half-life of ^{146}Sm compared to ^{147}Sm, ^{146}Sm-^{142}Nd, model ages are much less dependent than ^{147}Sm-^{143}Nd model ages on correctly accounting for fractionation of Sm from Nd that occurred during partial melting of the mare basalt source regions. For example, in the simplified model shown in Supplemental Figure 6, ages calculated using the ^{147}Sm-^{143}Nd isochron assuming the source regions have the same Sm/Nd as measured in the basalts shifts the age from 4.40 Gyr to 4.64 Gyr. In contrast, failure to account for fractionation of Sm from Nd during partial melting only shifts the ^{146}Sm-^{142}Nd model isochron age from 4.40 Gyr to 4.34 Gyr. Although not accounting for Sm/Nd fractionation during partial melting only shifts the ^{146}Sm-^{142}Nd isochron age by about 40 Myr, this is significantly more than typical uncertainties calculated using this system which can be as low as ~15 Myr.

One way to account for the Sm-Nd fractionation that occurs during melting is to calculate the source Sm/Nd ratio using the age and initial $^{143}Nd/^{144}Nd$ determined for individual basaltic samples. The equations for this approach are given in (Nyquist et al. 1995) and (Borg et al. 2016). Doing so turns this whole rock isochron approach into a model age because estimating the source Sm/Nd from the initial isotopic composition requires an assumption about the pre-formation evolution of the source; namely that the bulk Moon started from materials that evolved with chondritic Sm/Nd isotopic systematics prior to the event that formed the mare basalt source regions. Calculating the Sm/Nd of the mare basalt sources is done in an iterative fashion with each iteration progressively refining the age of the source region so that the age used to calculate the final Sm/Nd ratio is concordant with the age defined by the ^{146}Sm-^{142}Nd isochron (Borg et al., 2016).

This whole rock approach has the additional advantage that no assumption is necessary about the bulk Moon $^{142}Nd/^{144}Nd$ as this value is provided by the y-intercept of the ^{146}Sm-^{142}Nd isochron. For example, the whole rock ^{146}Sm-^{142}Nd isochron that contains data for both mare basalt sources and FAS minerals provides an age of 4.33 Gyr with an initial $^{142}Nd/^{144}Nd$ 15 ppm lower than the value determined in modern terrestrial basalts (Borg et al. 2019). Lunar evolution models that assume that the bulk-Moon has $\mu^{142}Nd$ of either -10, overlapping values seen in enstatite chondrites, or -20, overlapping values of ordinary chondrites, can match most of the initial $\varepsilon^{143}Nd$ and $\mu^{142}Nd$ data for the oldest lunar crustal rocks assuming LMO differentiation ages of 4.38 to 4.42 Gyr (Carlson et al. 2014).

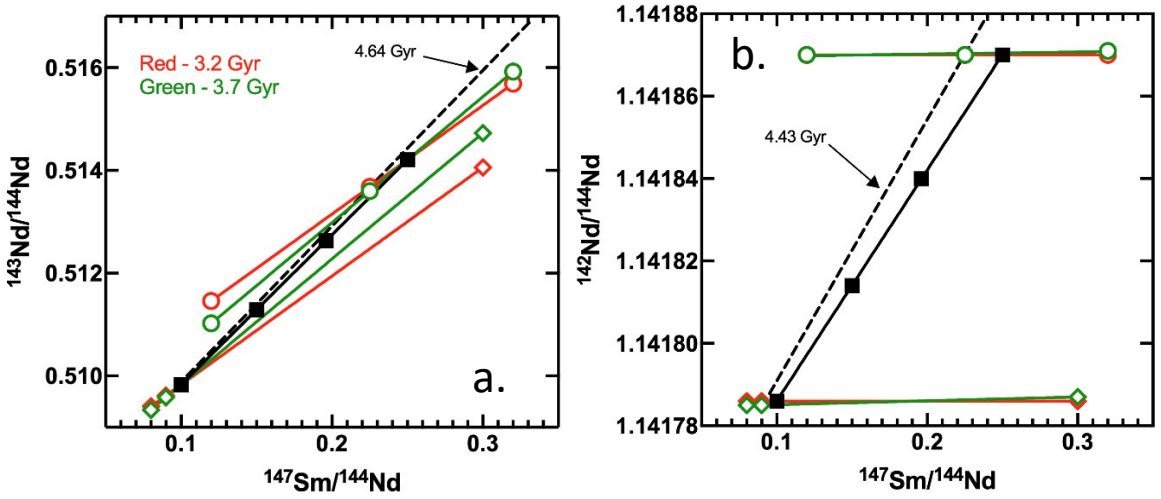

Supplemental Figure 6: Whole rock isochron diagrams for the ^{147}Sm-^{143}Nd and ^{146}Sm-^{142}Nd systems. The black squares on each diagram represent source regions for mare basalt magmas that formed at 4.40 Gyr and had identical ^{142}Nd/^{144}Nd and ^{143}Nd/^{144}Nd isotopic compositions at that time. They define the isochrons (black solid lines) with slopes that correspond to the 4.4 Gyr age. In this example, the source regions with the highest (circles) and lowest (diamonds) Sm/Nd are assumed to undergo melting events at 3.2 Gyr (red) or 3.7 Gyr (green) to produce magmas with Sm/Nd ratios 20% lower than that of their source. These magmas then crystallize minerals (open symbols) with both much higher and lower Sm/Nd than the whole rock. The minerals and their associated whole rocks define isochrons (colored lines) corresponding to the age of melting. These isochrons cross the 4.40 Gyr isochron at different points reflecting the different initial Nd isotopic compositions of the source of the magmas. Because of the change in Sm/Nd that occurs with melting, lines (dotted) fit through the 3.2 and 3.7 Gyr whole rocks define ages different from the true age of source formation, 4.64 Gyr for ^{147}Sm-^{143}Nd and 4.43 Gyr for ^{146}Sm-^{142}Nd. The lessened offset for the ^{146}Sm-^{142}Nd system reflects the short half-life of this system (103 Myr) compared to ^{147}Sm (106 Gyr). By 3.7 Gyr ^{146}Sm is essentially extinct as indicated by the nearly horizontal mineral isochrons on the right hand figure, so the change in Sm/Nd due to melting has little effect on the ^{142}Nd/^{144}Nd ratio.

LITERATURE CITED

Alibert C, Norman MD, McCulloch MT. 1994. An ancient Sm-Nd age for a ferroan noritic anorthosite clast from lunar breccia 67016. *Geochim. Cosmochim. Acta.* 58:2921-6

Barboni M, Boehnke P, Keller B, Kohl IE, Schoene B, et al. 2017. Early formation of the Moon 4.51 billion years ago. *Sci. Adv.*3:e1602365

Blichert-Toft J, Zanda B, Ebel DS, Albarede F. 2010. The Solar System primordial lead. *Earth Planet. Sci. Lett*. 300:152-63

Borg LE, Brennecka GA, Symes SJ. 2016. Accretion timescale and impact history of Mars deduced from the isotopic systematics of martian meteorites. *Geochim. Cosmochim. Acta* 175:150-67

Borg LE, Connelly JN, Boyet M, Carlson RW. 2011. Chronological evidence that the Moon is either young or did not have a global magma ocean. *Nature* 477:70-3

Borg LE, Connelly JN, Cassata WS, Gaffney AM, Bizzarro M. 2017. Chronologic implications for slow cooling of troctolite 76535 and temporal relationships between the Mg-suite and the ferroan anorthosite suite. *Geochim. Cosmochim. Acta* 201:377-91

Borg LE, Gaffney AM, Kruijer TS, Marks NA, Sio CK, Wimpenny J. 2019. Isotopic evidence for a young lunar magma ocean. *Earth Planet. Sci. Lett.* 523:115706

Borg LE, Gaffney AM, Shearer CK. 2015. A review of lunar chronology revealing a preponderance of 4.34-4.37 Ga ages. *Meteor. Planet. Sci.* 50:715-32

Borg LE, Norman M, Nyquist LE, Bogard DD, Snyder GA, et al. 1999. Isotopic studies of ferroan anorthosite 62236: a young lunar crustal rock from a light rare-earth-element-depleted source. *Geochim. Cosmochim. Acta* 63:2679-91

Bottke WF, Walker RJ, Day JMD, Nesvorny D, Elkins-Tanton L. 2010. Stochastic late accretion to Earth, the Moon, and Mars. *Science* 330:1527-30

Bouvier A, Vervoort JD, Patchett PJ. 2008. The Lu–Hf and Sm–Nd isotopic composition of CHUR: Constraints from unequilibrated chondrites and implications for the bulk composition of terrestrial planets. *Earth Planet. Sci. Lett.* 273:48-57

Boyet M, Carlson RW. 2007. A highly depleted moon or a non-magma ocean origin for the lunar crust? *Earth Planet. Sci. Lett.* 262:505-16

Boyet M, Carlson RW, Borg LE, Horan M. 2015. Sm-Nd systematics of lunar ferroan anorthosite suite rocks: constraints on lunar crust formation *Geochim. Cosmochim. Acta* 148:203-18

Boyet M, Gannoun A. 2013. Nucleosynthetic Nd isotope anomalies in primitive enstatite chondrites. *Geochim. Cosmochim. Acta* 121:652-66

Brandon AD, Lapen TJ, Debaille V, Beard BL, Rankenburg K, Neal C. 2009. Re-evaluating $^{142}Nd/^{144}Nd$ in lunar mare basalts with implications for the early evolution and bulk Sm/Nd of the Moon. *Geochim. Cosmochim. Acta* 73:6421-45

Burkhardt C, Borg LE, Brennecka GA, Shollenberger QR, Dauphas N, Kleine T. 2016. A nucleosynthetic origin for the Earth's anomalous ^{142}Nd composition. *Nature* 537:394-8

Carlson RW, Garcon M, O'Neil J, Reimink J, Rizo H. 2019. The nature of Earth's first crust. *Chem. Geo.* 530:119321

Carlson RW, Borg LE, Gaffney AM, Boyet M. 2014. Rb-Sr, Sm-Nd and Lu-Hf isotope systematics of the lunar Mg-suite: the age of the lunar crust and its relation to the time of Moon formation. *Philos. Trans. Roy. Soc. Lond*. A372

Carlson RW, Boyet M, Horan M. 2007. Chondrite barium, neodymium, and samarium isotopic heterogeneity and early earth differentiation. *Science* 316:1175-8

Carlson RW, Lugmair GW. 1988. The age of ferroan anorthosite 60025: oldest crust on a young Moon? *Earth Planet. Sci. Lett.* 90:119-30

Cherniak DJ. 2003. REE diffusion in feldspar. *Chem. Geo.* 193:25-41

Cherniak DJ, Liang Y. 2007. Rare earth element diffusion in natural enstatite. *Geochim. Cosmochim. Acta* 71:1324-40

Connelly JN, Bollard J, Bizzarro M. 2017. Pb-Pb chronometer and the early Solar System. *Geochim. Cosmochim. Acta* 201:345-63

Dodson MH. 1973. Closure temperature in cooling geochronological and petrological systems. *Contrib. Min. Petro*. 40:259-74

Fukai R, Yokoyama T. 2017. Neodymium isotope heterogeneity of ordinary and carbonaceous chondrites and the origin of non-chondritic 142Nd compositions in the Earth. *Earth Planet. Sci. Lett.* 474:206-14

Gaffney AM, Borg LE. 2014. A young solidification age for the lunar magma ocean. *Geochim. Cosmochim. Acta* 140:227-40

Gaffney AM, Borg LE, Asmerom Y, Shearer CK, Burger PV. 2011. Disturbance of isotope systematics during experimental shock and thermal metamorphism of a lunar basalt with implications for Martian meteorite chronology. *Meteor. Planet. Sci*. 46:35-52

Gannoun A, Boyet M, Rizo H, Goresy AE. 2011. 146Sm-142Nd systematics measured in enstatite chondrites reveals a heterogeneous distribution of 142Nd in the solar nebula. *Proceed. Nat. Acad. Sci.* 108:7693-7

Grange ML, Nemchin AA, Pidgeon RT, Muhling JR, Kennedy AK. 2009. Thermal history recorded by the Apollo 17 impact melt breccia 73217. *Geochim. Cosmochim. Acta* 73:3093-107

Grange ML, Nemchin AA, Timms N, Pidgeon RT, Meyer C. 2011. Complex magmatic and impact history prior to 4.1 Ga recorded in zircon from Apollo 17 South Massif aphanitic breccia 73235. *Geochim. Cosmochim. Acta* 75:2213-32

Hanan BB, Tilton GR. 1987. 60025: relict of primitive lunar crust? *Earth Planet. Sci. Lett.* 84:15-21

Kleine T, Munker C, Mezger K, Palme H. 2002. Rapid accretion and early core formation on asteroids and the terrestrial planets from Hf-W chronometry. *Nature* 418:952-5

Kleine T, Touboul M, Bourdon B, Nimmo F, Mezger K, Palme H, Jacobsen SB, Yin QZ., Halliday AN. 2009. Hf-W chronology of the accretion and early evolution of asteroids and terrestrial planets. *Geochim. Cosmochim. Acta.* 73:5150-88

Kruijer TS, Archer GJ, Kleine T. 2021. No ^{182}W evidence for early Moon formation. *Nature Geosci.* 14:714-15.

Kruijer TS, Kleine T. 2017. Tungsten isotopes and the origin of the Moon. *Earth Planet. Sci. Lett.* 475:15-24

Kruijer TS, Kleine T, Fischer-Godde M, Sprung P. 2015. Lunar tungsten isotopic evidence for the late veneer. *Nature* 520:534-7

Liu J, Touboul M, Ishikawa A, Walker RJ, Pearson DG. 2016. Widespread tungsten isotope anomalies and W mobility in crustal and mantle rocks of the Eoarchean Saglek Block, northern Labrador, Canada: implications for early Earth processes and W recycling. *Earth Planet. Sci. Lett.* 448:13-23

Lugmair GW, Scheinin NB, Marti K. 1975. Sm-Nd age and history of Apollo 17 basalt 75075: evidence for early differentiation of the lunar interior. *Proceed. 6th Lunar Sci. Conf.*: 1419-29

Marks NE, Borg LE., Shearer CK, and Cassata WS 2019. Geochronology of an Apollo 16 clast provides evidence for a basin-forming impact 4.3 billion years ago. *J. Geophys. Res. Planet.* 124:2465-2481

McCallum IS, Domeneghetti MC, Schwartz JM, Mullen EK, Zema M, et al. 2006. Cooling history of lunar Mg-suite gabbronorite 76255, troctolite 76535 and Stillwater pyroxenite SC-936: The record in exsolution and ordering in pyroxenes. *Geochim. Cosmochim. Acta* 70:6068-78

McCallum IS, O'Brien HE. 1996. Stratigraphy of the lunar highland crust: depths of burial of lunar samples from cooling-rate studies. *Am. Min.* 81:1166-75

McDougall I, Harrison TM. 1999. Geochronology and Thermochronology by the 40Ar/39Ar method. New York: Oxford University Press

McLeod CL, Brandon AD, Armytage RMG. 2014. Constraints on the formation age and evolution of the Moon from ^{142}Nd-^{143}Nd systematics of Apollo 12 basalts. *Earth Planet. Sci. Lett.* 396:179-89

Meyer C, Williams IS, Compston W. 1996. Uranium-lead ages for lunar zircons: evidence for a prolonged period of granophyre formation from 4.32 to 3.88 Ga. *Meteor. Planet. Sci.* 31:370-87

Mundl A, Touboul M, Jackson MG, Day JMD, Kurz MD, et al. 2017. Tungsten-182 heterogeneity in modern ocean island basalts. *Science* 356:66-9

Mundl A, Walker RJ, Reimink JR, Rudnick RL, Gashnig RM. 2018. Tungsten-182 in the upper continental crust: evidence from glacial diamictites. *Chem. Geo.* 494:144-52

Nemchin A, Timms N, Pidgeon R, Geisler T, Reddy S, Meyer C. 2009. Timing of crystallization of the lunar magma ocean constrained by the oldest zircon. *Nat. Geosci.* 2:133-6

Nemchin AA, Pidgeon RT, Whitehouse MJ, Vaughan JP, Meyer C. 2008. SIMS U-Pb study of zircon from Apollo 14 and 17 breccias: Implications for the evolution of lunar KREEP. *Geochim. Cosmochim. Acta* 72:668-89

Nemchin AA, Whitehouse MJ, Pidgeon RT, Meyer C. 2006. Oxygen isotopic signature of 4.4-3.9 Ga zircons as a monitor of differentiation processes on the Moon. *Geochim. Cosmochim. Acta* 70:1864-72

Nimmo F, Agnor CB. 2006. Isotopic outcomes of N-body accretion simulations: Constraints on equilibration processes during large impacts from Hf/W observations. *Earth Planet. Sci. Lett.* 243:26-43

Norman MD, Borg LE, Nyquist LE, Bogard DD. 2003. Chronology, geochemistry, and petrology of a ferroan noritic anorthosite clast from Descartes breccia 67215: clues to the age, origin, structure, and impact history of the lunar crust. *Meteor. Planet. Sci*. 38:645-61

Nyquist L, Bogard D, Yamaguchi A, Shih CY, Karouji Y, et al. 2006. Feldspathic clasts in Yamato-86032: Remnants of the lunar crust with implications for its formation and impact history. *Geochim. Cosmochim. Acta* 70:5990-6015

Nyquist LE, Shih C-Y, Wooden JL, Bansal BM, Wiesmann H. 1979. The Sr and Nd isotopic record of Apollo 12 basalts: implications for lunar geochemical evolution. *Proceed. 10th Lunar Planet. Sci. Conf.*: 77-114

Nyquist LE, Wiesmann H, Bansal B, Shih C-Y, Keith JE, Harper CL. 1995. ^{146}Sm-^{142}Nd formation interval for the lunar mantle. *Geochim. Cosmochim. Acta* 59:2817-37

Patterson C. 1956. Age of meteorites and the Earth. *Geochim. Cosmochim. Acta* 10:230

Pidgeon RT, Nemchin AA, Bronswijk WV, Geisler T, Meyer C, et al. 2007. Complex history of a zircon aggregate from lunar breccia 73235. *Geochim. Cosmochim. Acta* 71:1370-81

Puchtel IS, Blichert-Toft J, Touboul M, Horan MF, Walker RJ. 2016. The coupled ^{182}W-^{142}Nd record of early terrestrial mantle differentiation. *Geochem. Geophys. Geosys.* 17:2168-93

Puchtel IS, Blichert-Toft J, Touboul M, Walker RJ. 2018. ^{182}W and HSE constraints from 2.7 Ga komatiites on the heterogeneous nature of the Archean mantle. *Geochim. Cosmochim. Acta.* 228:1-26

Reimink JR, Chacko T, Carlson RW, Shirey SB, Liu J, et al. 2018. Petrogenesis and tectonics of the Acasta Gneiss Complex derived from integrated petrology and ^{142}Nd and ^{182}W extinct nuclide-geochemistry. *Earth Planet. Sci. Lett.* 494:12-22

Rizo H, Andrault D, Bennett N, Humayun M, Brandon A, et al. 2019. ^{182}W evidence for core-mantle interaction in the source of mantle plumes. *Geochem. Perspect. Lett.* 11:6-11

Rizo H, Walker R, Carlson RW, Touboul M, Horan M, et al. 2016. Early Earth differentiation investigated through ^{142}Nd, ^{182}W, and highly siderophile element abundances in samples from Isua, Greenland. *Geochim. Cosmochim. Acta* 175:319-336

Saji NS, Wielandt D, Holst JC, Bizzarro M. 2020. Solar system Nd isotope heterogeneity: insights into nucleosynthetic components and protoplanetary disk evolution. *Geochim. Cosmochim. Acta* 281:135-48

Sio CK, Borg LE, Cassata WS. 2020. The timing of lunar solidification and mantle overturn recorded in ferroan anorthosite 62237. *Earth Planet. Sci. Lett.* 538:116219

Snape JF, Nemchin AA, Bellucci JJ, Whitehouse MJ, Tartese R, et al. 2016. Lunar basalt chronology, mantle differentiation and implications for determining the age of the Moon. *Earth Planet. Sci. Lett.* 451:149-58

Snyder GA, Taylor LA, Halliday AN. 1994. Rb-Sr isotopic systematics of lunar ferroan anorthosite 62237 (abstr). Lunar and Planetary Science Conference 25:1309

Sprung P, Kleine T, Scherer EE. 2013. Isotopic evidence for chondritic Lu/Hf and Sm/Nd of the Moon. *Earth Planet. Sci. Lett.* 380:77-87

Sprung P, Scherer EE, Upadhyay D, Leya I, Mezger K. 2010. Non-nucleosynthetic heterogeneity in non-radiogenic stable Hf isotopes: Implications for early solar system chronology. *Earth Planet. Sci. Lett.* 295:1-11

Stacey JS, Kramers JD. 1975. Approximation of terrestrial lead isotope evolution by a two-stage model. *Earth Planet. Sci. Lett.* 26:207-21

Stoffler D, Ryder G, Ivanov BA, Artemieva NA, Cintala MJ, Grieve RAF. 2006. Cratering history and lunar chronology. *Rev. Min. Geochem.* 60:519-96

Tatsumoto M. 1970. Age of the Moon: an isotopic study of U-Th-Pb systematics of Apollo 11 lunar samples II. *Proceed. Apollo 11 Lunar Sci. Conf.:* 1595

Taylor DJ, McKeegan KD, Harrison TM. 2009. Lu-Hf zircon evidence for rapid lunar differentiation. *Earth Planet. Sci. Lett.* 279:157-64

Tera F, Papanastassiou DA, Wasserburg GJ. 1974. Isotopic evidence for a terminal lunar cataclysm. *Earth Planet. Sci. Lett.* 22:1-21

Tera F, Wasserburg GJ. 1972. U-Th-Pb systematics in lunar highland samples from the Luna 20 and Apollo 16 missions. *Earth Planet. Sci. Lett.* 17:36-51

Thiemens MM, Sprung P, Fonseca ROC, Leitzke FP, Munker C. 2019. Early Moon formation inferred from hafnium-tungsten systematics. *Nat. Geosci*. 12:696–700

Touboul M, Kleine T, Bourdon B, Palme H, Wieler R. 2007. Late formation and prolonged differentiation of the Moon inferred from W isotopes in lunar metals. *Nature*. 450:1206-9

Touboul M, Kleine T, Bourdon B, Palme H, Wieler R. 2009. Tungsten isotopes in ferroan anorthosites: implications for the age of the Moon and lifetime of its magma ocean. *Icarus* 199:245-9

Touboul M, Liu J, O'Neil J, Puchtel IS, Walker RJ. 2014. New insights into the Hadean mantle revealed by ^{182}W and highly siderophile element abundances in supracrustal rocks from the Nuvvuagittuq greenstone belt, Quebec, Canada. *Chem. Ge*o. 383:63-75

Touboul M, Puchtel IS, Walker RJ. 2015. Tungsten isotopic evidence for disproportional late accretion to the Earth and Moon. *Nature* 520:530-3

Touboul M, Puchtel IS, Walker RJ. 2012. ^{182}W evidence for long-term preservation of early mantle differentiation products. *Science* 335:1065-9

Unruh DM, Nakamura N, Tatsumoto M. 1977. History of the Pasamonte achondrite: relative susceptability of the Sm-Nd, Rb-Sr, and U-Pb systems to metamorphic events. *Earth Planet. Sci. Lett.* 37:1-12

Wendt I. Carl C. 1991. The statistical distribution of the mean squared weighted deviation. *Chem. Geol. Isotope Geosci. Sec.* 86:275-285

Willbold M, Elliott T, Moorbath S. 2011. The tungsten isotopic composition of the Earth's mantle before the terminal bombardment. *Nature* 477:195-8

Willbold M, Mojzsis SJ, Chen H-W, Elliott T. 2015. Tungsten isotope composition of the Acasta Gneiss Complex. *Earth Planet. Sci. Lett.* 419:168-77

Yin Q, Jacobsen SB, Yamashita K, Blichert-Toft J, Telouk P, Albarede F. 2002. A short timescale for terrestrial planet formation from Hf-W chronometry of meteorites. *Nature* 418:949-52

Supplemental Table 1. Summary of FAS Rb-Sr and Sm-Nd data

Sample	Initial $^{87}Sr/^{86}Sr$ at 4336 Ma	Sm-Nd Age (Myr)	Initial $\varepsilon^{143}Nd$	MSWD	Other concordant ages (Myr)	Weighted Average Age (Myr)
60016[a]	0.699060 ± 5	*4302 ± 28*	-0.28 ± 0.14	2.0	$4296^{+39}/_{-53}$ [j], 4275 ± 38 [k], 4311 ± 31 [l]	4304 ± 12
60025[b]	0.699055 ± 3	4367 ± 11	-0.24 ± 0.09	0.4	$4318^{+30}/_{-38}$ [j], 4359 ± 2 [m]	4360 ± 3
60025[c]	*0.699084 ± 20*	*4438 ± 38*	0.88 ± 0.68	4.6		
62236[d]	0.699020 ± 13	*4290 ± 85*	3.49 ± 0.98	4.7		
62237[e]	*0.699212 ± 12*	4350 ± 73	-0.53 ± 0.26	2.0		
62237[f]	0.699084 ± 17					
67016[g]	*0.699101 ± 8*	*4576 ± 160*	0.80 ± 0.60	6.5		
67215[h]	0.699084 ± 12	*4408 ± 130*	0.94 ± 0.76	34		
Y-86032[i]	0.699052 ± 10	4438 ± 34	0.19 ± 0.11	0.96		

All $^{87}Sr/^{86}Sr$ values normalized to NBS-987 = 0.710250. Weighted average initial $^{87}Sr/^{86}Sr$ = 0.699056 ± 11 (2 stdev; MSWD = 13). Number in italics not used in calculation.

[a.] Marks et al. (2019)

[b.] Borg et al. (2011)

[c.] Carlson & Lugmair (1988)

[d.] Borg et al. (1999)

[e.] Sio et al. (2020)

[f.] Snyder et al. (1994)

[g.] Alibert et al. (1994)

[h.]. Norman et al. (2003)

[i.] Nyquist et al. (2006)

[j.] ^{146}Sm-^{142}Nd age

[k.] Rb-Sr age

[l.] Ar-Ar age

[m.] Pb-Pb age

Supplemental Table 2 Compilation of Mg-suite ages

Sample	Age (Myr)	Chronometer	Initial $\varepsilon^{143}Nd$	MSWD	Average Age (Myr)
76535	4307 ± 11	^{147}Sm-^{143}Nd	-0.15 ± 0.22	1.5	4304 ± 10
	4295 ± 29	^{146}Sm-^{142}Nd		2.2	
	4308 ± 45	^{87}Rb-^{87}Sr		N/A[a]	
	4253 ± 58	^{147}Sm-^{143}Nd	0.16 ± 0.33	1.1	
	4330 ± 64	^{147}Sm-^{143}Nd	-1.25 ± 0.43	0.88	
	4301 ± 83	^{147}Sm-^{143}Nd	0.88 ± 0.53	14	
	4566 ± 60	*^{87}Rb-^{87}Sr*		*2.4*	
77215					
	4348 ± 80	^{146}Sm-^{142}Nd	-0.14 ± 0.05	0.1	4364 ± 38
	4375 ± 69	^{147}Sm-^{143}Nd	0.59 ± 0.39	1.0	
	4364 ± 55	^{87}Rb-^{87}Sr		5.4	
	4283 ± 23	*^{147}Sm-^{143}Nd*	*-0.54 ± 0.09*	*3.4*	
78236/8					
	4359 ± 24	^{87}Rb-^{87}Sr		0.27	4341 ± 15
	4332 ± 18	^{207}Pb-^{206}Pb		0.06	
	4334 ± 34	^{147}Sm-^{143}Nd	-0.27 ± 0.74	13	
	4333 ± 59	^{207}Pb-^{206}Pb		16000	
	4328 ± 59	^{147}Sm-^{143}Nd	1.54 ± 0.94	12	
	4436 ± 51	*^{147}Sm-^{143}Nd*	*-0.55* ± 0.45	*2.6*	
67667					
	4349 ± 31	^{147}Sm-^{143}Nd	0.03 ± 0.10	1.6	4351 ± 27
	4368 ± 67	^{87}Rb-^{87}Sr		1.9	
	4337 $^{+66}/_{-120}$	^{146}Sm-^{142}Nd		1.3	
	4176 ± 61	*^{147}Sm-^{143}Nd*	*0.82* ± 0.96	*1.2*	
15445 Clast B					4331 ± 69 [b]
	4334 ± 79	^{147}Sm-^{143}Nd	1.1 ± 1.9	2.4	
	4320 $^{+82}/_{-196}$	$^{142}Nd/^{143}Nd$		5.2	
	4291 ± 91	^{147}Sm-^{143}Nd	-0.35 ± 0.31	0.2	
	4470 ± 70	*^{147}Sm-^{143}Nd*	*0.72* ± 0.27	*1.4*	
Whole Rock A14, A15, A16, A17)	4348 ± 25	^{146}Sm-^{142}Nd	-0.24 ± 0.31	1.4	
15455, 228	4545 ± 150	^{87}Rb-^{87}Sr		3.6	
74217	4528 ± 92	^{87}Rb-^{87}Sr		4.1	
72255	4161 ± 89	^{87}Rb-^{87}Sr		4.0	
73255	4246 ± 48	^{147}Sm-^{143}Nd	0.72 ± 0.53	14	

Data compiled in Borg et al. (2015) and from Gaffney et al. (2015), Borg et al. (2017, 2020), Zhang et al (2021). Ages in italics are outlines and not included in the weighted means. [a.] Two-point tie line. [b.] Average based on only 2 ages.